Max-Planck-Institut
für Meteorologie

MAX-PLANCK-GESELLSCHAFT

International Max Planck Research School
on Earth System Modelling

Impact of Inhomogeneities on non-linear Cloud Processes

Torsten Weber

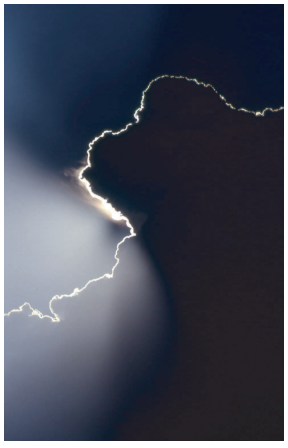

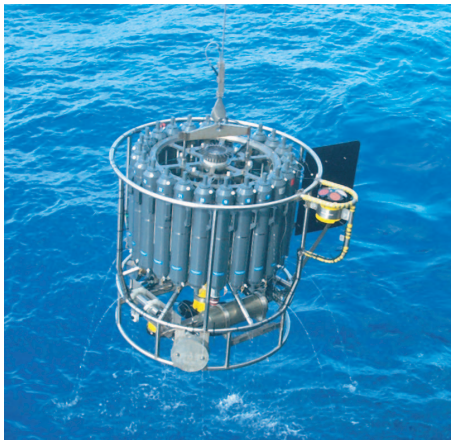

Berichte zur Erdsystemforschung 89/2011

Reports on Earth System Science

Hinweis

Die Berichte zur Erdsystemforschung werden vom Max-Planck-Institut für Meteorologie in Hamburg in unregelmäßiger Abfolge herausgegeben.

Sie enthalten wissenschaftliche und technische Beiträge, inklusive Dissertationen.

Die Beiträge geben nicht notwendigerweise die Auffassung des Instituts wieder.

Die "Berichte zur Erdsystemforschung" führen die vorherigen Reihen "Reports" und "Examensarbeiten" weiter.

Notice

The Reports on Earth System Science are published by the Max Planck Institute for Meteorology in Hamburg. They appear in irregular intervals.

They contain scientific and technical contributions, including Ph. D. theses.

The Reports do not necessarily reflect the opinion of the Institute.

The "Reports on Earth System Science" continue the former "Reports" and "Examensarbeiten" of the Max Planck Institute.

Anschrift / Address

Max-Planck-Institut für Meteorologie
Bundesstrasse 53
20146 Hamburg
Deutschland

Tel.: +49-(0)40-4 11 73-0
Fax: +49-(0)40-4 11 73-298
Web: www.mpimet.mpg.de

Layout:

Bettina Diallo, PR & Grafik

Titelfotos:
vorne:
Christian Klepp - Jochem Marotzke - Christian Klepp
hinten:
Clotilde Dubois - Christian Klepp - Katsumasa Tanaka

Berichte zur Erdsystemforschung 89/2011

Impact of Inhomogeneities on non-linear Cloud Processes

Torsten Weber

aus Lübeck

Hamburg 2011

Reports on Earth System Science 89/2011

ISSN 1614-1199

Torsten Weber
Max-Planck-Institut für Meteorologie
Bundesstrasse 53
20146 Hamburg
Germany

Als Dissertation angenommen
vom Department Geowissenschaften der Universität Hamburg

auf Grund der Gutachten von
Prof. Dr. Martin Claußen
und
Dr. Johannes Quaas

Hamburg, den 25. Januar 2011
Prof. Dr. Jürgen Oßenbrügge
Leiter des Departments für Geowissenschaften

ISSN 1614-1199

Impact of Inhomogeneities on non-linear Cloud Processes

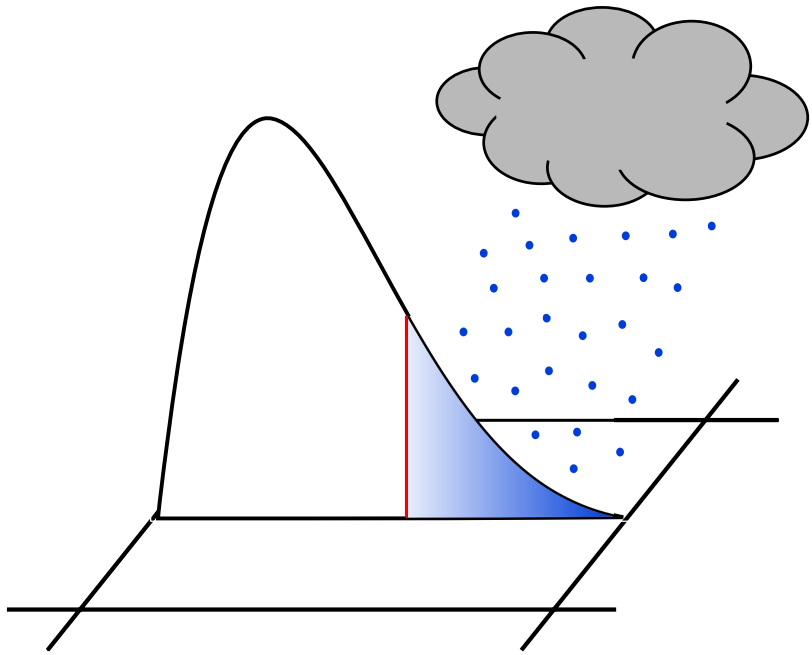

Torsten Weber

Hamburg 2011

Contents

Abstract

The deficiencies in parameterizations of subgrid-scale processes, such as cloud processes, are one important source of uncertainties in modeled climate scenarios. Neglecting subgrid-scale horizontal variability of clouds introduces biases to all non-linear cloud processes, e.g., formation of clouds and precipitation formation. In order to reduce these biases, a prognostic parameterization for the subgrid-scale variability of water vapor and cloud condensate was implemented by Tompkins (2002) in the ECHAM5 climate model. The scheme uses a probability density function (PDF) of the total water mixing ratio to calculate the horizontal cloud fraction. The PDF used here is a beta-distribution whose variance (distribution width) and skewness (shape-parameter q) are prognostic variables in the model and evolve as a function of atmospheric processes such as turbulence, convection, and large-scale cloud microphysical processes.

In this study, the cloud cover scheme was evaluated using data of the Moderate Resolution Imaging Spectroradiometer (MODIS) satellite instrument. The results show that the mean total water path (TWP) and the mean cloud cover are on average relatively well simulated. However, large deficiencies are revealed by the evaluation of both variance and skewness of the PDF. Systematically negative deviations of variance were found for almost all regions of the globe. Skewness of the TWP is strongly overestimated in the Tropics, and underestimated in the extratropical regions. Sensitivity tests were made to improve the parameterization of variance and skewness. Improved results were obtained with the distribution width increased by reducing the dissipation caused by horizontal and vertical eddies. In particular, the large positive bias in skewness in the Tropics could be reduced by modifying the influence of deep convection on the PDF. Moreover, some model experiments were carried out to allow for negative skewness in the cloud cover scheme. Especially, the modeled skewness in the Tropics could be improved through the combination of allowing negative skewness, reducing the dissipation of distribution width caused by vertical eddies, calculating skewness increase only for detrainment from ice-containing deep convection and generally increasing positive skewness (shape-parameter q) by 20%.

In the second part of this work, the impact of the subgrid-scale variability of cloud liquid water on the autoconversion process was investigated. For this purpose, the statistical PDF approach was incorporated in a continuous autoconversion parameterization. Thus, the revised autoconversion rate is calculated by an integral of the autoconversion equation over the PDF of total water mixing ratio from the saturation vapor mixing ratio to the maximum of total water mixing ratio. An evaluation of the new autoconversion parameterization was carried out by means of a one year simulation with the ECHAM5 climate model. The results indicate that the new autoconversion scheme causes an increase of occurrence in autoconversion for higher rates and a decrease for lower ones compared to the original scheme. This can be explained by the applied PDF of total water mixing ratio which emphasizes areas of high cloud liquid water and the non-linearity of the autoconversion with respect to liquid water mixing ratio. A similar trend as in the autoconversion was observed in the accretion process resulting from the coupling of both processes. As a consequence of the altered autoconversion, large-scale surface precipitation also shows a shift of occurrence from lower to higher rates. Moreover, the affected vertically integrated cloud liquid water, total cloud cover, cloud radiative forcing and total precipitation estimated by the model are

compared with observational data derived from ground based measurements and satellite instruments, showing slight improvements. The artificial “tuning” factor for autoconversion could be reduced by almost an order of magnitude.

Zusammenfassung

Defizite in der Parametrisierung von subskaligen Wolkenprozessen stellen eine der größten Ursachen von Unsicherheiten in simulierten Klimaszenarien dar. Die Vernachlässigung der subskaligen Variabilität von Wolken führt zu Fehlern in allen nicht-linearen Wolkenprozessen wie z. B. Wolken- oder Niederschlagsbildung. Um diese Fehler zu reduzieren, wurde von Tompkins (2002) eine prognostische Parametrisierung dieser subskaligen Variabilität in das ECHAM5 Klimamodell implementiert. Das Schema verwendet eine Wahrscheinlichkeitsdichtefunktion (PDF) des Gesamtwassermischungsverhältnisses, um die horizontale Wolkenbedeckung zu berechnen. Die Varianz (Verteilungsbreite) und Schiefe (Formparameter q) der Verteilung sind prognostische Variablen im Modell und werden durch atmosphärische Prozesse wie Turbulenz, Konvektion und subskalige mikrophysikalische Wolkenprozesse beeinflusst.

In dieser Studie wurde das Wolkenbedeckungsschema unter Verwendung von hochaufgelösten Daten des Moderate Resolution Imaging Spectroradiometer (MODIS) Instruments evaluiert. Die Ergebnisse zeigen, dass der mittlere Gesamtwasserweg und die mittlere Wolkenbedeckung relativ gut vom Modell simuliert werden. Große Unzulänglichkeiten dagegen wurden durch die Untersuchung sowohl in der simulierten Varianz als auch der Schiefe der PDF aufgedeckt. Systematische negative Abweichungen der Varianz sind für fast alle Regionen auf dem Globus gefunden worden. Die Schiefe des Gesamtwasserweges wird in den Tropen stark überschätzt, in den außertropischen Regionen dagegen unterschätzt. Darüber hinaus wurden Sensitivitätstests durchgeführt, um die atmosphärischen Prozesse zu identifizieren, welche zu großen Fehlern in der Varianz und Schiefe beitragen.

Die zu geringe modellierte Verteilungsbreite kann durch eine Reduzierung der Dissipation von Verteilungsbreite durch horizontale und vertikale Wirbel verbessert werden. Besonders die große positive Abweichung der Schiefe in den Tropen kann durch eine Modifizierung des Einflusses der hochreichenden Konvektion auf die PDF reduziert werden. Zusätzlich wurden in einigen Experimenten Änderungen in der Parametrisierung der Schiefe vorgenommen, um negative Schiefe im Wolkenschema zuzulassen. Insbesondere die modellierte Schiefe in den Tropen kann durch eine Kombination von Zulassen negativer Schiefe, Reduzierung der Dissipation von Verteilungsbreite durch vertikale Wirbel, Berechnung der Zunahme von Schiefe nur durch Ausmischung von Konvektion oberhalb des Gefrierniveaus und eine allgemeine Erhöhung der positiven Schiefe (Formparameter q) von 20% im Vergleich zu den Beobachtungsdaten verbessert werden.

Im zweiten Teil dieser Arbeit wurde der Einfluss der subskaligen Variabilität von Wolkenflüssigwasser auf den Autokonversionsprozess untersucht. Zu diesem Zweck ist der statistische PDF-Ansatz in die Autokonversionsparametrisierung implementiert worden. Die auf diese Weise überarbeitete Autokonversionsrate wird nun durch ein Integral der Autokonversionsgleichung über die PDF des Gesamtwassermischungsverhältnisses vom Sättigungsmischungsverhältnis des Wasserdampfs bis zum Maximum des Gesamtwassermischungsverhältnisses berechnet. Eine Evaluation der neuen Autokonversionsparametrisierung wurde mittels einer Simulation eines Jahres mit dem ECHAM5 Klimamodell durchgeführt.

Die Ergebnisse zeigen, dass das neue Autokonversionsschema im Vergleich zur ursprünglichen Parametrisierung die Häufigkeit von hohen Autokonversionsraten erhöht und die Häufigkeit von kleineren Raten reduziert. Diese Veränderung kommt durch die Nichtlinearität der Autokonversion als Funktion des Wolkenflüssigwassers zustande, die Bereiche der Gitterbox mit besonders hohen Wolkenwassergehalten stärker gewichtet. Eine Verschiebung der Häufigkeit hin zu höheren Intensitäten wurde ebenfalls beim Akkreszenzprozess beobachtet, welche durch die Kopplung mit dem Autokonversionsprozess in der Modell-Parametrisierung hervorgerufen wird. Aufgrund der geänderten Autokonversion zeigen auch die Raten des großskaligen Niederschlags eine Verschiebung hin zu höheren Intensitäten. Darüber hinaus werden in dieser Arbeit auch die durch die neue Parametrisierung beeinflussten Modellgrößen wie vertikal-integriertes Wolkenflüssigwasser, Gesamtwolkenbedeckung, Wolkenstrahlungsantrieb und Gesamtniederschlag mit boden- und satellitengestützten Beobachtungsdaten verglichen, welche teilweise nun besser vom Modell simuliert werden. Zusätzlich konnte durch die überarbeitete Parametrisierung der künstliche Tuning-Faktor in der Autokonversionsgleichung um fast eine Größenordnung verkleinert werden.

1. Introduction

1.1. Motivation

The climate system of the earth affects the life of humans in many fundamental ways. It determines the conditions for agriculture and usable water resources in the different regions being a precondition for settlements. Climate conditions are also responsible for the occurrence of natural hazards such as surges, droughts, storm and hurricane tracks damaging the environment. Thus, the understanding of the climate system and the ability to make projections for climate change are crucial prerequisites to develop strategies mitigating the negative impact on economy and society. The main tools for calculating projections for the future climate are general circulation models (GCMs) running on high performance computers.

Clouds constitute an important component of the climate system. They affect the radiation budget of the earth system through reflecting and absorbing the incoming shortwave (SW) and outgoing longwave (LW) radiation (Fig. 1.1). This process depends strongly on the radiative properties of clouds (e.g. content of liquid water, ice or both and particle size spectra) as well as on their geometry, thickness and occurrence in different heights in the atmosphere. Low level clouds, e.g. cumulus or stratocumulus, tend to cool the atmosphere scattering solar radiation strongly, since they are often optically thick, but emitting radiation characterized by their warm surface temperature at the top. The opposite effect is caused by high level clouds, e.g. cirrus or cirrustratus, emitting LW radiation back to the surface and the low layers of the atmosphere. At the same time they scatter less solar radiation since they are often optically thin. Mid-level clouds, e.g. altocumulus or altostratus, consist of both cloud liquid water and ice crystals, and are therefore also labeled mixed-phase clouds. Other kinds of mixed-phase clouds extending from the lower to the upper atmosphere can produce long lasting precipitation (nimbustratos clouds) and thunderstorms (cumulunimbus clouds).

Clouds play also a decisive role in the hydrological circle because they redistribute the energy vertically as a result of releasing latent heat by condensation and remove water from the atmosphere by precipitation formation (Fig. 1.1). The former process is governed by the humidity, temperature and the number of condensation nuclei of the air in which the cloud is embedded. Light precipitation such as drizzle (rain drops radius less than $0.25\ \mathrm{mm}$[1]) is produced in warm clouds (where the temperature is above zero) by coagulating cloud droplets (autoconversion) and collecting cloud droplets by falling rain drops (accretion). These clouds, also labeled as low stratiform clouds, occur very often in regions having low temperature surfaces and warm air in higher layers of the atmosphere (inversions). Such conditions are frequently given over the subtropical

[1] defined by AMS Glossary (Glickman, 2000)

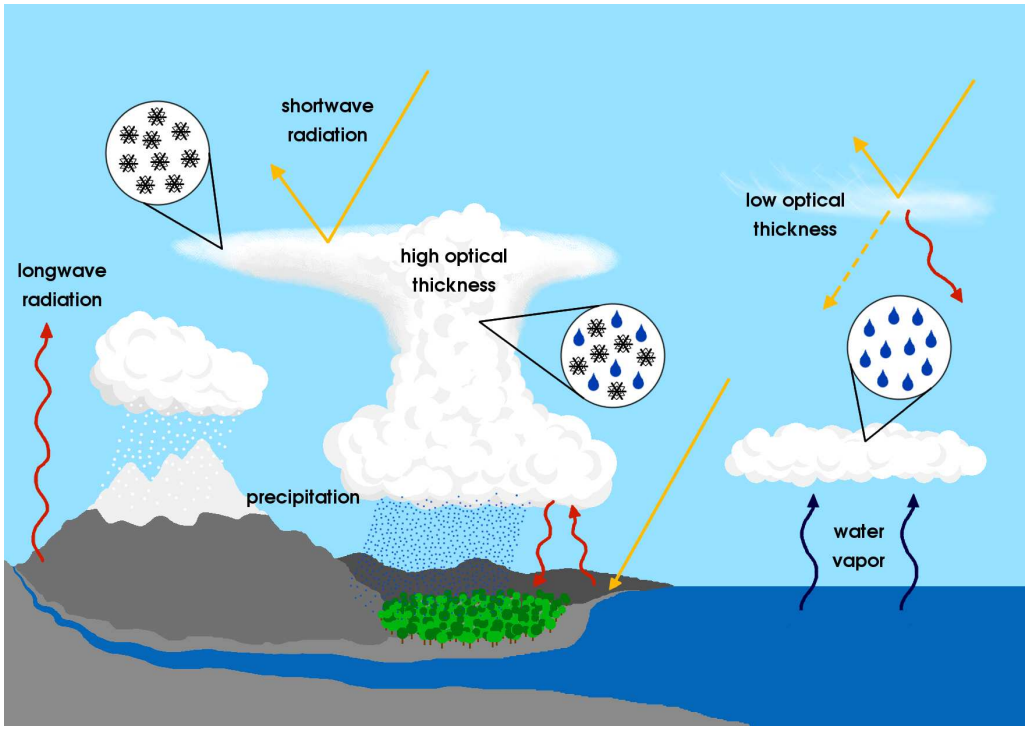

Figure 1.1.: The role of clouds in the climate system. They impact the radiation budget of the earth system in the solar (yellow arrows) and terrestrial (red arrows) spectra and play also a decisive role in the hydrological circle.

ocean on the western sides of the continents where cold currents from oceanic upwelling cool the lower atmosphere. In cold clouds, cloud droplets undergo a transition by heterogeneous (between 0°C and -32°C, determined by Doutriaux-Boucher and Quaas (2004)) and homogeneous (below -32°C) freezing to ice crystals. Snow can grow by aggregation of ice crystals and by collecting ice crystals and cloud droplets. The size of ice crystals, and consequently of snow, depends strongly on temperature and humidity supply, and becomes smaller the lower the temperatures are since then absolute humidity is low. The occurrence of the described processes generating different kinds of precipitation is coupled with the presence of clouds which should therefore be modeled accurately in GCMs.

The different representation of clouds in GCMs is one of the largest sources for uncertainties in modeled climate scenarios. Dufresne and Bony (2008) revealed that the standard deviation resulting from the cloud-climate feedback accounts for nearly 70% of the standard deviation of the total temperature change in idealized climate change experiments. One major contribution to the afore-mentioned uncertainties is the neglected subgrid-scale variability of clouds. In GCMs, grid-box mean values of variables are commonly used to calculate the cloud cover and cloud microphysics. This assumption introduces biases as high as a factor of two to all non-linear cloud processes, such as precipitation formation and radiation (Pincus and Klein, 2000). To reduce these biases, certain parameters in cloud process parameterizations such as autoconversion have to be "tuned" to unrealistic values to obtain realistic results (Rotstayn, 2000).

A new statistical approach potentially reduces the bias in the non-linear cloud processes taking into account the horizontal subgrid-scale variability of water vapor and cloud condensate introduced in the cloud cover scheme of the ECHAM5 climate model (Tompkins, 2002). A probability density function (PDF) of total water mixing ratio is used to calculate the horizontal cloud fraction in a model grid-box by an integral of the PDF from the saturation vapor mixing ratio to infinity (see Section 2.2 for more details).

In this thesis, the statistical cloud cover scheme in ECHAM5 is evaluated by means of satellite data to reveal possible discrepancies between the modeled and observed subgrid-scale distribution of water. An analysis of the subgrid-scale distribution of vertically integrated total water on a global scale is carried out using data of the Moderate Resolution Imaging Spectroradiometer (MODIS) satellite instrument. Moreover, sensitivity experiments are made to analyze the parameterization of atmospheric processes affecting the variance and skewness of the PDF. After this evaluation of the cloud cover scheme, the subgrid-scale variability of cloud liquid water is introduced in the precipitation formation in warm clouds. To achieve this, the current autoconversion parameterization derived by Beheng (1994) in the ECHAM5 climate model is revised incorporating the statistical PDF approach by Tompkins (2002). In model experiments, the impact of the incorporated subgrid-scale variability scheme on the autoconversion of cloud droplets as well as the accretion process (raindrops collecting cloud droplets) and affected quantities (total cloud cover, cloud liquid water, cloud radiative forcing and precipitation) is analyzed. Furthermore, the results are compared with observational data from MODIS, the Energy Balanced and Filled (EBAF) product of the Clouds and the Earth's Radiant Energy System (CERES), the Global Precipitation Climatology Project (GPCP) as well as the Hamburg Ocean Atmosphere Parameters and Fluxes from Satellite Data (HOAPS) to asses the achieved improvements.

1.2. Model Description

For this study the atmospheric general circulation model ECHAM5 developed at the Max Planck Institute for Meteorology is used. A detailed description of the model physics was published by Roeckner et al. (2003). In this section, the components of the model, which are relevant for the simulation of cloud processes, are briefly summarized. The model contains a spectral dynamical core calculating the vorticity, temperature, divergence and logarithm of surface pressure in the horizontal by a truncated series of spherical harmonics with triangular truncation at wavenumbers 21, 31, 42, 63, 85, 106 or 159. In the vertical direction, a hybrid coordinate system with 19 or 31 levels and an uppermost computational level at 10 hPa can be applied in the standard configuration. In this work, the horizontal resolutions T42 with 19 vertical levels and T63 with 31 vertical levels are used to analyze the impact of inhomogeneities on non-linear cloud processes. The tracer transport is simulated by means of a semi-Lagrangian scheme (Lin and Rood, 1996) which affects the water components (vapor, liquid and solid) as well.

Stratiform clouds are described by a scheme consisting of prognostic equations for the vapor, liquid and ice phase by Lohmann and Roeckner (1996). The horizontal cloud fraction is determined by a statistical cloud cover scheme using a beta-function based PDF of total water mixing ratio

(Tompkins, 2002). Its shape is affected by convection, turbulence and microphysical cloud processes simulated by prognostic equations for the distribution moments. Thus, the cloud fraction for each grid-box is calculated by an integral over the saturated part of the PDF (see Section 2.2 for more details). The total cloud cover in a model column is diagnosed by the maximum-random overlap assumption. The microphysics scheme considers the transition of water through condensation, evaporation, freezing and melting, as well as the deposition of water vapor and sublimation of snow and ice in the cloudy part of the grid-box. It also takes into account the sedimentation of cloud ice, evaporation of falling rain and melting of snow.

The precipitation formation in warm ($\mathrm{T} > 0\ \mathrm{C}^\circ$) and mixed phase clouds ($-35\ \mathrm{C}^\circ <= \mathrm{T} < 0\ \mathrm{C}^\circ$) is governed by the formation of raindrops by coagulating cloud droplets (autoconversion) and the increase in rainwater mass due to raindrops collecting cloud droplets (accretion). The autoconversion rate and the accretion rate are derived from the stochastic collection equation, which describes the time evolution of a droplet spectrum changing by collisions among droplets of different size (Beheng, 1994). The accretional growth of snow by collecting cloud droplets is described by Lin et al. (1983) and Levkov et al. (1992). Moreover, the precipitation scheme is able to distinguish between maritime and continental clouds by considering the cloud droplet number concentration. In cold clouds, the accretional growth of snow by collecting ice crystals (Lin et al., 1983; Levkov et al., 1992) and the conversion from cloud ice to snow by aggregation of ice crystals (Levkov et al., 1983; Murakami, 1990) are taken into account. The precipitation generated by the aforementioned processes is labeled as large-scale precipitation in the model. Cumulus convection and convective precipitation are simulated by a mass flux scheme (Tiedke, 1989) with modifications for deep convection according to Nordeng (1994). This scheme considers the mass, heat, moisture, cloud water and momentum for cumulus updrafts and downdrafts, and provides the cloud water detrainment as source term for the stratiform cloud water equations. An adjustment-type closure for deep convection is applied with the convective potential energy (CAPE) as parameter for the convective activity (Nordeng, 1994).

The radiation scheme in the model contains an algorithm for the SW and LW radiative transfer. SW radiation is calculated for four different spectral bands, one for the visible and ultraviolet range, and three for the near infrared range. The scheme follows the work of Fouquart and Bonnel (1980) and uses the Eddington approximation for the integration over the zenith and azimuth angles and the delta-Eddingtion approximation for the reflectivity of a layer. Rayleigh scattering, absorption by water vapor and ozone as well as a uniformly mixed gas ($\mathrm{CO_2} + \mathrm{N_2O} + \mathrm{CO} + \mathrm{CH_4} + \mathrm{O_2}$) are included. The LW radiation scheme follows the Rapid Radiative Transfer Model (RRTM) (Mlawer et al., 1997) and uses the correlated-k method applied to 16 spectral bands, and includes the line absorption by $\mathrm{H_2O}$, $\mathrm{CO_2}$, $\mathrm{O_3}$, $\mathrm{CH_4}$, CFC11, CFC12, CFC22 and aerosols.

Turbulent fluxes at the surface for moisture, heat and momentum are described by the bulk transfer relation, which considers the difference between the lowest model level and the surface of the respective variable affected by the horizontal wind vector and a transfer coefficient. The coefficient is determined from the Monin-Obukhov similarity theory by integrating the flux-profile relations over the lowest model layer. Above the surface layer, the eddy diffusion method is used accounting for the vertical gradient of the respective variable which is correlated to its turbulent flux. The land surface temperature is derived from the surface energy balance equation applying an implicit coupling scheme (Schulze et al., 2001) to calculate the respective prognostic variables and surface fluxes.

2. Evaluation of the Statistical Cloud Cover Scheme in ECHAM5

A modified version of this chapter was submitted to the Q. J. R. Meteorol. Soc. in October 2010.

2.1. Introduction

The accurate representation of clouds in GCMs requires a proper theoretical concept of cloud microphysics and dynamic processes which result from fluctuations of humidity and temperature on the one hand as well as preferably a high resolution model grid on the other hand. But, for practical applications, there is a need for a compromise of accuracy and computational capacity. The simplest approach to simulate non-convective cloud formation in a GCM is to employ a relative humidity threshold above which fractional cloudiness is diagnosed. An often used relationship between cloud cover and relative humidity as predictor was described by Sundqvist et al. (1989). Other cloud schemes applying the relative humidity threshold were improved by additional predictors such as the vertical velocity to parameterize low level clouds associated with extratropical fronts and tropical disturbances (Slingo, 1987) or the cloud water content to estimate the stratiform components of total cloud amount (Xu and Randall, 1996). Pincus and Klein (2000) found that by accounting for the subgrid-scale variability in microphysical processes in cloud schemes, the bias in the non-linear process rates caused by using averaged quantities can be reduced and arbitrary tuning of parameters can also be avoided.

One approach to take the spatial variability of clouds into account is to describe the respective quantity in the grid-box in terms of a PDF. Early statistical schemes which applied this innovative concept were developed by Sommeria and Deardorff (1977) and Mellor (1977). They used a joint PDF for the subgrid-scale liquid potential temperature and total water content to estimate the cloud fraction by integrating over the saturated part of the PDF. This concept implies that the saturated part of the PDF condenses immediately and the chosen PDF shape is able to reproduce the spatial distribution of the total water content. Several observational studies were carried out to analyze the shape of distributions for humidity related quantities in different conditions. Wood and Field (2000) found complex and often bimodal PDFs of total water content having large values of skewness in data from flights through stratocumulus clouds, which capped a well-mixed planetary boundary layer (PBL) or were decoupled from it. Similar results for PDFs of liquid water content being bimodal as well as positively and negatively skewed were reported by Davis et al. (1996) measured during flights through marine stratocumulus clouds. Moreover, in the PBL, various shapes of humidity-distributions such as gaussian, skewed, platykurtic, and multimodal were

identified by Price (2001) examining data from tethered-balloon measurements. The studies show that the shape of the observed quantity varies a lot depending on the environmental conditions. Therefore, the choice of the assumed shape of the humidity-distribution is one crucial criteria for a successful performance of a statistical PDF scheme.

The simplest form of a PDF based on a symmetric uniform distribution is used by Le Treut and Li (1991) to describe the sum of water vapor and cloud condensate in a grid-box. A similar approach was made by Smith (1990) who uses a relative humidity threshold function derived from a symmetric triangular PDF diagnosing the variance of cloud water content. This simple condensation scheme was adopted by Rotstayn (1997) and Nishizawa (2000). It is evident that these simple PDFs are not able to reproduce the spatial distribution of the respective quantity in all cases, but they are easy to handle and have a low computational cost. The beta-function, which is employed by Tompkins (2002), provides a more flexible approach to represent the spatial distribution of total water mixing ratio. Other comprehensive concepts were developed by Watanabe et al. (2009), who use double-uniform and skewed-triangular distributions in different conditions for temperature and total water content fluctuations, and Golaz et al. (2002) applying a joint PDF of a double-gaussian function of vertical velocity, liquid water potential temperature and total specific water content to characterize the unresolved subgrid variations in a grid-box.

Another important aspect is how the statistical moments of a PDF are determined and which atmospheric processes affect the development of the distribution moments. The number of parameters to define a PDF depends on the shape of the distribution. In more advanced schemes, the higher moments such as variance and skewness or alternatively the lower and upper limits of the distribution are calculated by means of prognostic equations. However, in some PDF schemes, the number of prognostic equations is reduced by setting the higher order moments constant in order to decrease the complexity of scheme. LeTreut and Li (1991) fixed the variance of total water in their cloud generation scheme to a value of 20% of total water to obtain a good agreement between the observed and simulated mean zonal cloudiness, for instance. But, Tompkins (2008) showed that PDF schemes having a fixed variance are equivalent to the specification of the critical relative humidity concept developed by Sundqvist et al. (1989). Accordingly, to exploit the complete skills of statistical PDF schemes, it is preferable to formulate prognostic equations for all defining quantities of the distribution. This means that the prognostic equations should take into account the dynamic and turbulent processes as well as the microphysics affecting the shape of the PDF.

Now new, high spatial resolution (of order of $5 \times 5\ \mathrm{km}^2$) retrievals of column water vapor and column cloud condensate are available from satellites globally. These observational data allow construction of horizontal PDFs at the much coarser resolution of typical GCMs. Unfortunately, the data with high spatial resolution only allow for the retrieval of vertically integrated total water (total water path, TWP), while instruments providing vertically resolved water vapor and cloud condensate mixing ratio retrievals (such as infrared sounders) still have spatially too coarse resolutions (of order of $20 \times 20\ \mathrm{km}^2$ and more) to allow construction of PDFs.

This chapter presents an evaluation of the subgrid-scale variability scheme of total water mixing ratio developed and implemented by Tompkins (2002) in the ECHAM5 climate model. In detail, the defining parameters of the PDF, the modeled mean of TWP, its variance and skewness as well

as the total cloud cover are compared with high spatial resolution satellite data. Moreover, an analysis of the parameterized processes (e.g. turbulence and convective detrainment) which affect the variance and skewness is carried out. Initially, in Section 2.2, the subgrid-scale variability scheme of total water is summarized, and in Section 2.3, the model experiments and the methods to analyze the model and satellite data are explained. Afterwards, the results of the comparison between the modeled quantities and the ones derived from MODIS and the results of sensitivity experiments are presented in Section 2.4. The evaluation closes with a summary of the results and conclusion in Section 2.5.

2.2. Subgrid-Scale Variability Scheme in ECHAM5

The ECHAM5 climate model (Roeckner et. al, 2003) employs a statistical-dynamical approach to account for the subgrid-scale variability of water vapor and cloud condensate which was developed by Tompkins (2002). It uses the prognostic equations of the water phases (vapor, liquid and solid) and the bulk cloud microphysics described by Lohmann and Roeckner (1996). The subgrid-scale variability scheme neglects the temperature fluctuation within a model grid-box assuming the subgrid-scale formation of clouds is caused only by fluctuations in the total water mixing ratio. Then, the horizontal cloud cover C can be calculated by

$$C = \int_{r_s}^{\infty} G(r_t) dr_t, \tag{2.1}$$

where saturation vapor mixing ratio r_s is assumed to be constant within the considered grid-box and $G(r_t)$ represents a PDF of the total water mixing ratio r_t, the sum of water vapor, cloud liquid water and cloud ice. Accordingly, the covered part of the grid-box is equal to the integral of the total water mixing ratio from the saturation value to infinity if $G(r_t)$ is normalized to one (Fig. 2.1). The, the mean cloud condensate $\overline{r}_c$ can be expressed by

$$\overline{r}_c = \int_{r_s}^{\infty} (r_t - r_s) G(r_t) dr_t. \tag{2.2}$$

Analysis of the run from a cloud resolving model (CRM) with a horizontal resolution of 350 m and 50 vertical levels revealed that the beta-distribution gives a good fit to the distribution of total water mixing ratio (Tompkins, 2002). The beta-distribution is defined through the shape-parameters p and q which govern the skewness, and the lower and upper limits a and b. The PDF is given by

$$G(r_t) = \frac{1}{B(p,q)} \frac{(r_t - a)^{p-1} (b - r_t)^{q-1}}{(b-a)^{p+q-1}}, \tag{2.3}$$

with

$$B(p,q) = \frac{\Gamma(p)\Gamma(q)}{\Gamma(p+q)}, \tag{2.4}$$

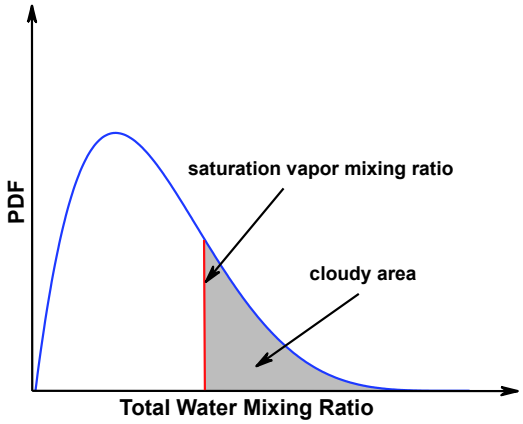

Figure 2.1.: PDF of total water mixing ratio. The grey shaped area represents the cloudy part of the grid-box and is equal to the integral of the PDF from the saturation vapor mixing ratio to infinity.

for $a \leq r_t \leq b$, $p > 0$, $q > 0$ and Γ as the gamma function. Thus, mean of total water mixing ratio is calculated integrating the PDF of total water mixing ratio from its minimum to its maximum:

$$\overline{r}_t = \frac{1}{B(p,q)} \int_a^b \frac{r_t (r_t - a)^{p-1} (b - r_t)^{q-1}}{(b-a)^{p+q-1}} dr_t. \tag{2.5}$$

Eq. (2.5) can be solved trough the coordinate transformation $y = (r_t - a)/(b - a)$:

$$\overline{r}_t = (b-a)\frac{p}{p+q} + a. \tag{2.6}$$

Applying the similar method for the mean water vapor $\overline{r}_v$ and the mean cloud condensate $\overline{r}_c$ gives:

$$\begin{aligned} \overline{r}_v =& (b-a)\frac{p}{p+q} I_x(p+1,q) \\ &+ (a - r_s) I_x(p,q) + r_s, \end{aligned} \tag{2.7}$$

$$\begin{aligned} \overline{r}_c =& (b-a)\frac{p}{p+q} [1 - I_x(p+1,q)] \\ &+ (a - r_s)[1 - I_x(p,q)], \end{aligned} \tag{2.8}$$

where the incomplete beta-function ratio I_x with $x = (r_s - a)/(b - a)$ is expressed as:

$$I_x(p,q) = \frac{1}{B(p,q)} \int_0^x t^{p-1} (1-t)^{q-1} dt. \tag{2.9}$$

Finally, the horizontal cloud cover can be determined by

$$C = 1 - I_x(p,q). \tag{2.10}$$

Atmospheric processes such as turbulence and microphysics affect the moments of the distribution of total water mixing ratio and therefore the defining parameters. Due to simplifications in the current version of the subgrid-scale variability scheme p is set constant equal 2 and q is allowed to assume values between 2 and 50. As a result of this relation of p and q, the distribution of total water mixing ratio can only be bell-shaped ($p = q$) or positively skewed ($p < q$), where the skewness ς is given by

$$\varsigma = \frac{2(q-p)}{p+q+2}\sqrt{\frac{p+q+1}{pq}} \tag{2.11}$$

and the variance υ is written as follows:

$$\upsilon = \left(\frac{b-a}{p+q}\right)^2 \frac{pq}{p+q+1}. \tag{2.12}$$

In the model, the temporal evolution of the shape-parameter q is calculated by the following prognostic equation:

$$\begin{aligned}\frac{Dq}{Dt} =& \frac{K}{\overline{\rho} r_s}\frac{\partial}{\partial z}(M^{cu} r_c^{cu}) + \frac{\Delta q^{micro}}{\Delta t} \\ &+ (q_0 - q)\left(\frac{1}{\tau_v} + \frac{1}{\tau_h}\right).\end{aligned} \tag{2.13}$$

The first term of Eq. (2.13) is related to convection and describes the increase of skewness through detrainment of cloud condensate, where K denotes a dimensionless constant which specifies how quickly detraining water from convection increases the skewness, $\overline{\rho}$ is the mean air density, M^{cu} is the updraft mass flux, r_c^{cu} represents the mean cloud water in the convective updrafts, and q_0 defines the shape of the final distribution. The present scheme neglects the impact of convective downdrafts so that the skewness is restricted in the turbulent PBL resulting in limited vertical gradients. Consequently, vertical transport of skewness by vertical turbulence is also neglected. Microphysical processes taking place in clouds are regarded in the second term. A reduction of the cloud condensate $\Delta\overline{r}_c^{micro}$ caused by precipitation or evaporation, for instance, reduces the maximum of total water mixing ratio b and accordingly the shape-parameter q and shifts the PDF towards a symmetric shape. Both variables are coupled through the equation of the mean of total water mixing ratio (2.6) which is expressed as

$$\Delta q^{micro} = \frac{\left[b + \frac{\Delta\overline{r}_c^{micro}}{\overline{r}_c}(b - r_s) - a\right] p}{\overline{r}_t - a} - (p+q). \tag{2.14}$$

Turbulence is taken into account in the third term using a Newtonian relaxation which drives the distribution in presence of mixing towards a symmetric one. Omitting the horizontal terms of the equation for the change of distribution width (DW) concerning the subgrid-scale velocity fluctuations, the dissipation timescale divided into a horizontal τ_h and vertical component τ_v is

written as:

$$\tau_v = \frac{\kappa l}{\sqrt{e}} \text{ with } l = \frac{kz}{1 + kz/\lambda}, \tag{2.15}$$

$$\tau_h^{-1} = C_s^2 \sqrt{\left(\frac{\partial u}{\partial x}\right)^2 + \left(\frac{\partial v}{\partial y}\right)^2}. \tag{2.16}$$

Eq. (2.15) describes the dissipation caused by 3D turbulence in the PBL and in the vicinity of deep convection cores, where κ is a constant, e the turbulent kinetic energy, k the von Kármán's constant, z the height and λ the asymptotic mixing length. Eq. (2.16) represents the dissipation through large-scale 2D horizontal eddies due to horizontal wind shear instability with the horizontal wind components u and v, and C_s^2 is a constant.

In addition to the Eq. (2.13) for the skewness (represented by the shape-parameter q), the mean total water mixing ratio and the mean cloud condensate already provided by the model are needed to close the system. The variance, or the width of the PDF, can then be diagnosed. However, in certain cases, when clear sky occurs ($\overline{r}_c = 0$) or in overcast conditions ($\overline{r}_v \geq \overline{r}_s$), the system is not closed and a further equation is required. To solve this problem, Tompkins (2002) decided to apply an additional quasi-prognostic equation that estimates the DW ($b - a$) of total water mixing ratio being proportional to its variance:

$$\begin{aligned} \frac{D(b-a)}{Dt} =& \frac{(\overline{r}_t - a)(p + q + \Delta q_{conv})p^{-1} - (b-a)}{\Delta t} \\ & - \frac{\eta}{(b-a)} \overline{w' r_t'} \frac{\partial \overline{r}_t}{\partial z} - \Lambda \sqrt{e} \frac{\partial (b-a)}{\partial z} \\ & - (b-a) \left(\frac{1}{\tau_v} + \frac{1}{\tau_h} \right). \end{aligned} \tag{2.17}$$

The first term of Eq. (2.17) takes into account the effect of deep convection detrainment on the DW, where Δq_{conv} is equal to the first term on the right hand side of Eq. (2.13). The second term of Eq. (2.17) estimates the production of DW when a vertical moisture gradient exists with $\eta = (p+q)^2(p+q+1)(pq)^{-1}$ and $\overline{w' r_t'}$ as the turbulent moisture flux including the vertical wind w. Vertical transport of DW through subgrid eddies is described in the next term, where $\Lambda = l S_r$ and S_r is a stability function, and the last term describes the impact of dissipation.

2.3. Data and Methodology

2.3.1. Model Simulations

The parameterization prognostically computing the subgrid-scale PDF of total water mixing ratio was developed by Tompkins (2002) and implemented in the ECHAM5 GCM (Roeckner et al., 2003). For evaluation of this cloud cover scheme, the year 2004 (as characterized by the prescribed sea ice and sea surface temperatures) was simulated with the ECHAM5 model starting three months earlier to reach an equilibrium for the cloud microphysical processes. Two different model experiments were carried out using the resolutions T42L19 and T63L31, which have a horizontal resolution of about 313 km and 208 km at the equator, and 19 and 31 vertical levels respectively with the uppermost pressure level at 10 hPa. As boundary conditions for the model experiments, the observed monthly mean sea surface temperature and sea ice data of 2004 were used as in the Atmospheric Model Intercomparison Project (AMIP, Gates et al., 1999). The variables considered in this study are the grid-box mean of TWP, its variance (distribution width) and skewness (shape-parameter q) as well as the total cloud cover calculated every hour. While Tompkins (2002) uses the DW ($b - a$) in his scheme, here the variance (υ) is employed because the calculation of variance is less sensitive to outliers in the reference observational data and is therefore more robust. Furthermore, to compare the modeled shape-parameter q with the skewness of TWP derived from satellite data, it was necessary to convert the shape-parameter q to the skewness of TWP. The model mean total water mixing ratio (i.e. vertically resolved), its variance and skewness could not be compared with satellite data directly since these data are available only as a vertical integral on a two-dimensional grid. Firstly, the grid-box mean of total water mixing ratio $\overline{r}_t$ was determined for each model level adding the variables water vapor, cloud liquid water and cloud ice. Subsequently, the total water mixing ratio, its minimum a and maximum b were vertically integrated under the assumption of maximum overlap (see section 2.5 for discussion). These variables were used to diagnose the shape-parameter q by means of the rearranged Eq. (2.6). Finally, the calculation of the skewness ς and variance υ were carried out using Eq. (2.11) and (2.12). However, because of the vertical integration of TWP and the approximately exponential profile of water vapor, which exhibits the largest amount in the lower atmosphere, the TWP is mainly dominated by the planetary boundary layer humidity. Consequently, the variance and skewness derived from the TWP after its vertical integration are also mainly affected by the lower atmosphere.

2.3.2. Satellite Data

In order to evaluate the scheme, the observational data set L2 Joint Product of MODIS on the Terra satellite (Platnick et al., 2003; King et al., 2003) was employed for the year 2004. Its high spatial resolution of 5×5 km^2 permits to capture the horizontal spatial subgrid-scale variability of column water vapor and cloud condensate very well at the much coarser model resolution of T42, with up to 3844 MODIS retrievals within one T42 model grid-box. As MODIS does not provide the TWP in one variable, the instantaneous retrievals of water vapor (Precipitable Water Infrared Clear) and condensed water (Cloud Water Path) including cloud ice had to be used. To obtain

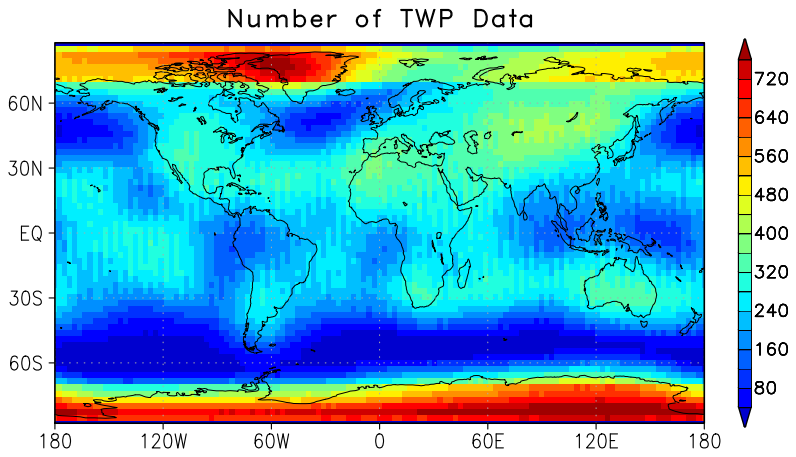

Figure 2.2.: Number of grid-boxes with TWP data from the reduced MODIS dataset.

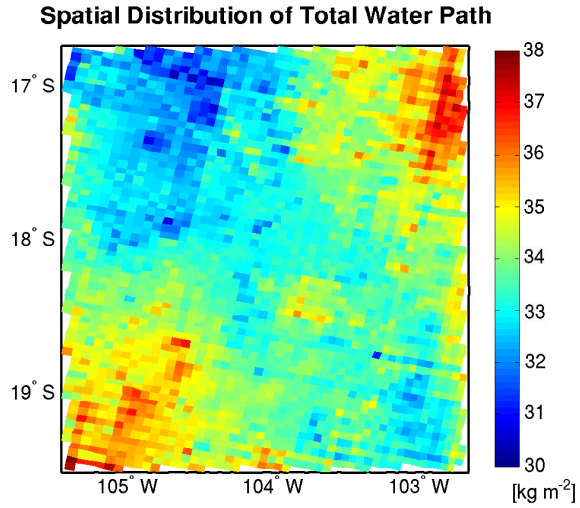

Figure 2.3.: Spatial distribution of TWP in an example model grid-box filled with MODIS data pixels.

reliable retrievals of water vapor, only data pixels were selected where the Cloud Mask of MODIS indicates “confident clear” or “probably clear” sky. The occurring gaps in the images due to clouds or missing retrievals were filled by a linear interpolation of the 8 nearest data pixels when at least 25% of the scene was cloud-free. If less than 25% of a scene was cloud-free, then the MODIS image was discarded from the analysis. Linear interpolation was applied under the assumption that the water vapor in columns containing clouds similar is to the concentration in surrounding clear skies. While this assumption is probably not strictly correct, it is considered good enough for this statistical analysis. The chosen threshold level of 25% is the result of a compromise between having enough data pixel for the interpolation and obtaining a large number of images (filled grid-boxes) for a reliable statistical analysis especially in those regions where cloudy conditions prevail.

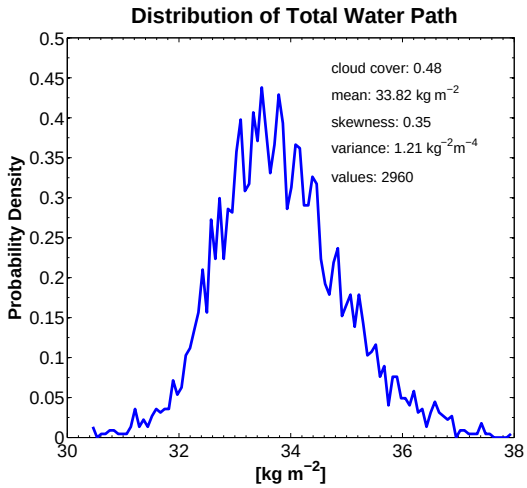

Figure 2.4.: Observation-derived distribution of TWP from the model grid-box in Fig. 2.3 and the corresponding statistics.

For instance, using this threshold, about 40% of the images were rejected due to this constraint, compared to a 50% threshold excluding out 79%. It is assumed that the large number of grid-boxes, from which the statistical quantities were calculated, reduce the impact of potential errors caused by the interpolation. A similar selection process was applied to the images of condensed cloud water using the Water Path Confidence Quality Assurance of MODIS. Moreover, only data pixels of the condensed water image were selected which possess a "very good confidence" or a "good confidence". Finally, the reduced dataset of water vapor and condensed cloud water of each image were added together to form the TWP. The number of grid-boxes with TWP data from the reduced MODIS dataset is shown in Fig. 2.2. As expected, the number of data is rather small in regions characterized by large cloud cover, in particular over the southern oceans around 60°S, but very high in the Polar regions caused by more overlapping satellite swaths and estimated clear skies by MODIS.

In contrast to the model data, which is available globally and at hourly intervals, the MODIS data was recorded along the satellite swath at solar local time. Thus, this data had to be assigned to the model grid-boxes by means of the latitude/longitude information and time (+/- 30 minutes; i.e., one model time-step) of the data pixels. Additionally, only model grid-boxes were selected containing at least 100 MODIS data pixels in order to obtain reliable results of variance and skewness (Fig. 2.3). Afterwards, the statistical parameters of TWP (mean, its variance and skewness) were estimated from each grid-box as shown exemplarily in Fig. 2.4 and the mean deviations of these quantities (model minus MODIS) were calculated. The total cloud cover was derived from the Cloud Mask of MODIS. Furthermore, one has to keep in mind that because of the measurement method of MODIS, the TWP and its derived statistic parameters mainly represent the lower atmosphere as explained in the section of the model data.

2.4. Results

2.4.1. Model vs. Observation

To compare the model results and observations, the relative mean error and the root mean square error (RMS) of the deviations of total cloud cover, TWP, and its variance and skewness were calculated (Tab. C.1/ C.3). Furthermore, the spatial deviations of these parameters are displayed for the resolution T42L19 at a 0.95 significance level using a two-sided t-test (Figs. 2.5a-d). For comparison the annual mean values of analyzed quantities derived by MODIS are shown in Figs. 2.5e-h.

The modeled total cloud cover differs with a relative mean error of 3.2% and an RMS of 0.14 from the MODIS data which has a mean cloud cover of 0.63. Looking at the geographic regions one can reveal the processes leading to the discrepancies. Fig. 2.5a shows an underestimation of total cloud cover by the model mainly over the oceans, in particular, off the western coasts of the continents, and an overestimation of clouds in high latitudes, over Africa and South America as well as over the central Pacific. Negative deviations on the western sides of the continents, where usually stratocumulus clouds prevail, indicate that the cloud cover scheme has a deficiency in simulating this type of shallow marine boundary-layer clouds. Positive deviations over North Africa, Antarctica and the North Pole region, however, might be caused by a systematic underestimation of clouds in the MODIS data rather than model errors, because it is difficult for satellite instruments to detect clouds in regions which exhibit bright surfaces such as ice, snow or sand.

A marginally better agreement to the observational data is found in the TWP with a relative mean error of 1.3% referring to MODIS mean of 26.55 $\mathrm{kg\,m^{-2}}$ and an RMS of 3.34 $\mathrm{kg\,m^{-2}}$. In detail, the deviation patterns are quite similar to the ones of the total cloud cover. The modeled TWP is mostly too low over the oceans on the western sides of the continents as well as over Indonesia and Australia, and too high over the central Pacific, South Africa, Asia and between $60°\mathrm{S}-45°\mathrm{S}$ over the southern oceans (Fig. 2.5b). These deviations may be attributed to deficiencies in the hydrological cycle of the model. The regions in the north of $60°\mathrm{N}$ and south of $60°\mathrm{S}$ as well as North Africa and Arabia show also positive deviations of TWP, but because of the afore-mentioned uncertainties in the MODIS data, these deviations are excluded from the interpretations of their origins. However, evaluation of the mean values has been done earlier (e.g. Chen et al., 1996) and is not of central interest to this study.

The third analyzed quantity, the variance, is globally underestimated by the model which can be seen in the large relative mean error of -82% referring to the MODIS mean of 7.56 $\mathrm{kg^2\,m^{-4}}$ and the RMS of 10.15 $\mathrm{kg^2\,m^{-4}}$. Particularly, large differences to the observations are found in the low latitudes, and over the continents potentially indicating deficiencies in the turbulence parameterization (Fig. 2.5d). However, higher deviations towards the equator suggests that, additionally, a humidity related process is not well described or does not work properly in the cloud cover scheme. One possible explanation could be that the precipitation process removes too much liquid water out of the clouds resulting in a too low variance. But, it has to be mentioned that because of the coupling of variance (distribution width) and skewness (shape-parameter q) through Eq. (2.17), the flawed skewness also contributes to the errors of the variance (for more details see

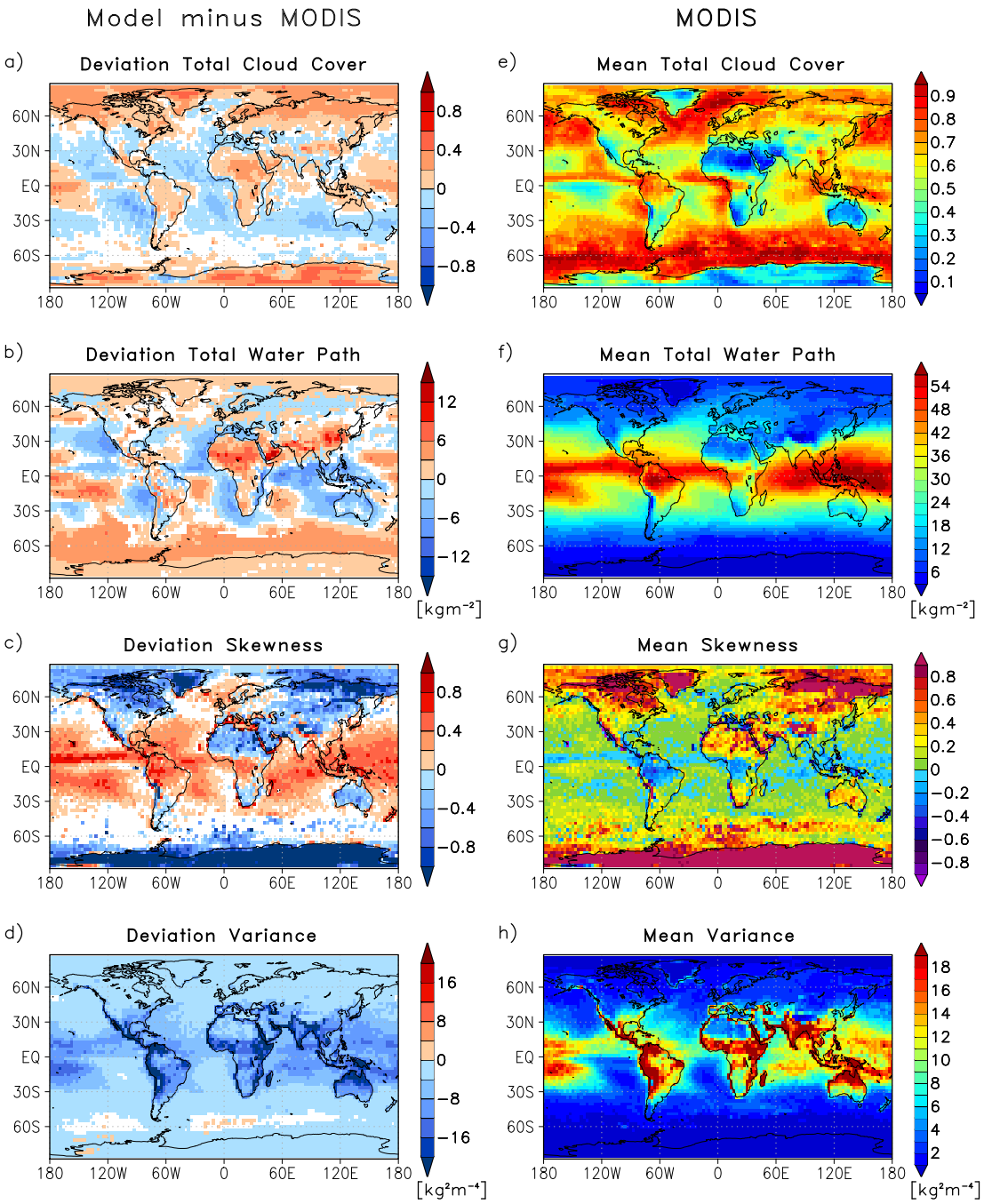

Figure 2.5.: Left column depicts the deviation of modeled annual mean total cloud cover, TWP and its skewness and variance (T42L19) from MODIS data (white areas mask out differences not significant at a 0.95 statistical significance level) and the right column shows the annual mean values derived from MODIS of 2004.

section 2.4.2). Furthermore, an analysis of the frequency of cloud cover in the model experiment T63L31 indicates that the prognostic equation for variance (distribution width) is applied in 90.3% of the cases (clear sky or overcast) and diagnosed in only 9.7% of the cases (partly covered). This suggests that the prognostic equation for variance (distribution width) contributes more to the bias than diagnostic closure of the equation system.

Deviations of the skewness of TWP are geographically differently distributed than the quantities analyzed before. The model strongly overestimates the skewness in the Tropics and over the oceans as well as, to a lesser extent, over Europe. It underestimates the skewness over North America, South Africa, continental Asia and Australia. Despite the large deviations of skewness shown in Fig. 2.5c, the relative mean error of 5% compared to the MODIS mean of 0.20 is fairly low. This results from the positive and negative deviations almost compensating for each other. Accordingly, it is more reasonable to rely on the RMS of 0.49 or try to separate the regions with different signs of deviations. If the analysis is confined to the region between $30°\mathrm{S}-30°\mathrm{N}$, the RMS decreases to 0.40 and the relative mean error increases to 460%. One reason for these large positive errors is certainly that only positive skewness is allowed in the model whereas the data derived from MODIS exhibits negative skewness, especially in the Tropics (Fig. 2.5g). Negative skewness can be caused by strong convective downdrafts which transport dry air from upper layers to lower ones or into the PBL. Neglecting these downdrafts as done in the prognostic equation for skewness in the model may also contribute to the above mentioned errors. In general, the discrepancy between skewness and the observational data is likely to be caused by shortcomings in the cloud cover scheme's link to the convection parameterization of the cloud cover scheme.

The results of the evaluation of the higher model resolution T63T31 are quite similar to the described deviations of T42L19 both in the geographic patterns and in its RMS except for the variance for which RMS is 32.5% lower (Tab. C.1/C.3). Moreover, the large-scale cloud cover scheme by Sundqvist et. al (1989), based on a relative humidity threshold without a prognostic PDF, was also evaluated and compared with the PDF scheme in terms of the total cloud cover and the TWP. Only marginal differences in the RMS of T42L19 and small discrepancies in the relative mean errors of cloud cover are found in T63L31 resolutions. The disagreement with the observations of TWP are slightly lower in the PDF scheme both in the RMS and the relative mean errors.

2.4.2. Sensitivity Experiments

Sensitivity experiments were carried out to identify in detail the processes leading to the respective deviations of modeled variance and skewness of TWP from the observations and to potentially improve the agreement. In these experiments diabatic and dynamical processes increasing or decreasing variance and skewness, as parameterized by Tompkins (2002), were switched off or modified (an overview of the experiments can be seen in Tab. 2.1). Furthermore, some runs were made to reduce the deviation of the variance and skewness by combining the modifications of the single experiments and, additionally, allowing negative skewness in the model. Each sensitivity run compasses a simulation of the first three months of 2004 and was compared with MODIS measurements of the same time period.

Table 2.1.: Description of the sensitivity experiments

Experiment	Description	Intention
control	standard model setup	
vdiff	disabled vertical diffusion of DW of TWP	increase of variance
vedd	reduced dissipation of DW caused by vertical eddies by the factor of 10	increase of variance
hedd	reduced dissipation of DW caused by horizontal eddies by the factor of 10	increase of variance
rsk	calculating skewness of TWP only for deep convection	reduction of skewness
qmin	minimum of shape-parameter q is set to constant equal to 1	allowing negative skewness
pvar	shape-parameter p is set to vary as $p = (q+1)/(q-1)$	allowing negative skewness

In the first experiment (labeled *vdiff*) the vertical diffusion of DW was switched off with the intention to increase the mean variance. This process which transports the DW vertically is described in the third term of Eq. (2.17). However, the impact of dissipation on the variance is very small which can be seen in the RMS of 10.64 $\mathrm{kg}^2\,\mathrm{m}^{-4}$ compared to the RMS of 10.66 $\mathrm{kg}^2\,\mathrm{m}^{-4}$ for the control run. Consequently, the spatial pattern of this parameter shows only tiny changes in this run. A similarly low impact is observed in skewness indicating by its RMS (Tab. C.4) and its spatial pattern being almost identical to the ones of the run without modifications (figure not shown).

The next two experiments analyze the effect of dissipation caused by horizontal and vertical eddies on the DW (last term of Eq. (2.17)) reducing the influence by these processes by a factor of 10. In the first run (*hedd*), where the dissipation caused by horizontal eddies is mitigated, the deviation of the modeled variance from the observations is somewhat lower with an RMS of 10.54 $\mathrm{kg}^2\,\mathrm{m}^{-4}$, caused by an increase of variance in the Tropics. No remarkable changes in the spatial pattern result from this experiment in the skewness whose RMS of 0.73 is marginally higher than the one in the control run. In the second run (*vedd*), in which the dissipation caused by vertical eddies is reduced, the RMS of the variance decreases by 11.2% to 9.47 $\mathrm{kg}^2\,\mathrm{m}^{-4}$ induced by an increase of variance mainly over the oceans and in the Tropics (Fig. 2.6g). The modification of the dissipation leads also to an enhancement of skewness over the extra-tropical oceans (Fig. 2.6b) resulting in a marginally higher RMS of 0.73.

In the next three experiments the cloud scheme was modified for the purpose of decreasing the skewness especially in the Tropics. To achieve this, in the first run (*rsk*) only the detrainment by high-reaching convection (determined as convective clouds consisting of ice rather than liquid

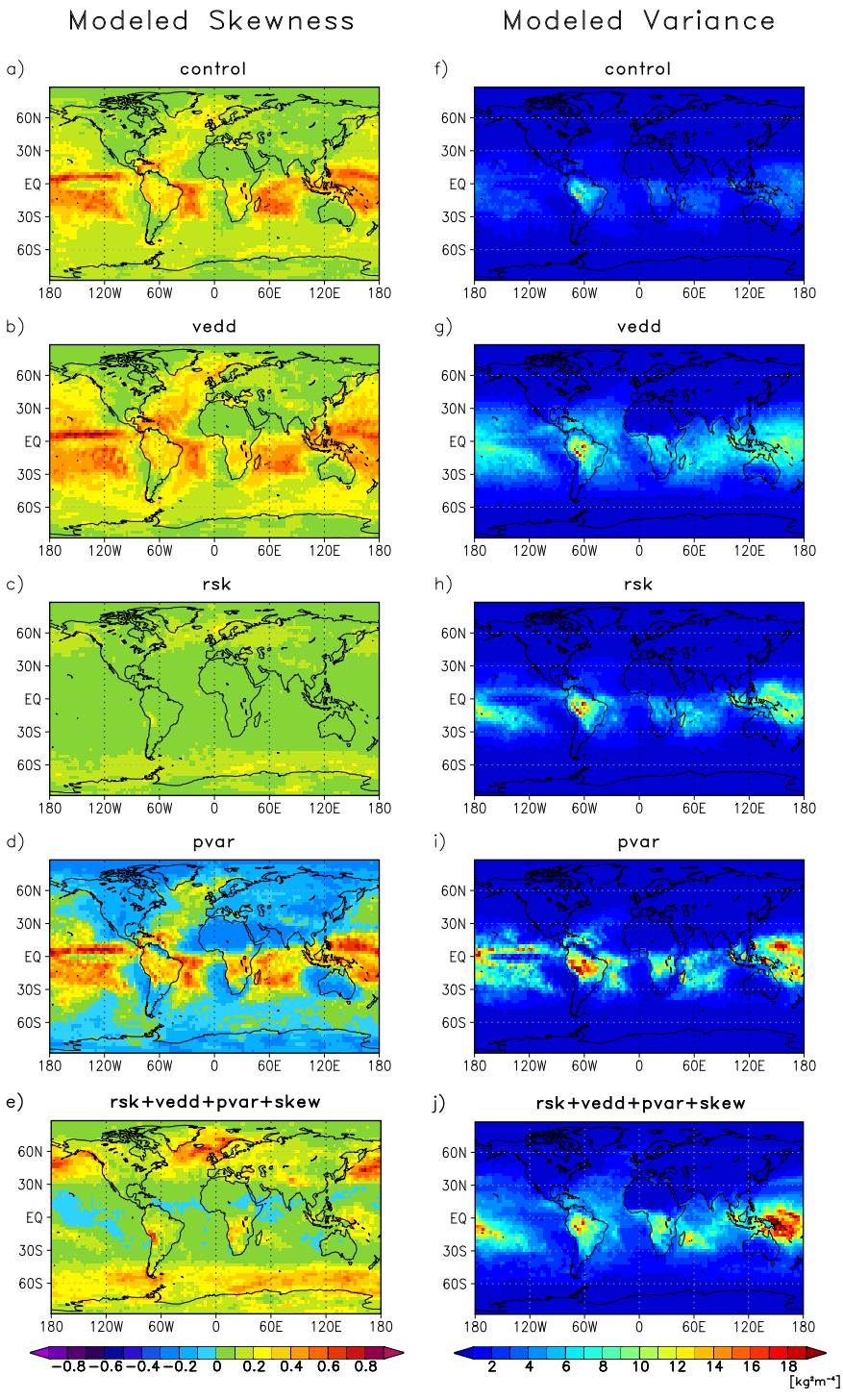

Figure 2.6.: Left column shows the modeled skewness and the right column the modeled variance of simulations with different paramterizations for the resolution T42L19 (mean of three months of 2004). The abbreviations of the experiments are explained in Tab. 2.1.

water) was allowed to increase the skewness of total water mixing ratio (first term of Eq. (2.13)). Its result shows a strong reduction of skewness in the low latitudes and a band of higher positive values around 60° South and North compared to the control run (Fig. 2.6c). Such significant changes in the spatial pattern of skewness, however, have only consequences in the RMS which decreases only slightly by 4.2% from 0.72 to 0.69, whereas the relative mean error increases from -31% to -79.3%. This seems curious but it is explained by disappearing of high skewness values in the low latitudes and thus less cancellation of errors. It becomes even more obvious if the area for calculation of the deviation errors is confined to 30°S to 30°N. Then the relative mean error decreases from 333.3% of the control run to -50% in the modified run and the RMS of 0.44 to 0.30 which is a decline of 31.8%. The impact of the modified calculation of skewness on the variance is only weak indicated by a somewhat lower RMS of 10.05 $\mathrm{kg}^2\ \mathrm{m}^{-4}$ and its retained spatial pattern (Fig. 2.6h).

Although the pattern of skewness in the experiment *rsk* is closer to the MODIS measurements, there is a lack of negative values in the modeled skewness. To solve this problem it is necessary to allow for negative skewness in the model. In the general case, this would require an additional prognostic equation for the shape-parameter p. In order to avoid this, Tompkins (2008) suggests to let the shape-parameter p be tied to q and vary as $p = (q+1)/(q-1)$, which allows for relations of p and q leading to negative skewness. The result of this modified parametrization (*pvar*) causes a decline of skewness in regions where already low positive values exist to negative ones but the spatial pattern of skewness is maintained (Fig. 2.6d). Consequently, the RMS of skewness increases to 0.81. A better result shows the RMS of the variance of 9.77 $\mathrm{kg}^2\ \mathrm{m}^{-4}$ induced by an increase of variance in the low latitudes (Fig. 2.6i). Another possibility to generate negative skewness without adding a further prognostic equation is to reduce the lower limit of q to one enabling cases where p can be larger than q. However, this experiment (*qmin*) leads to even lower negative values keeping the spatial pattern as in the experiment *pvar* and increases the RMS to 0.92 (figure not shown).

The RMS of the total cloud cover is almost equal to the one of the control run in the afore-analyzed experiments (Tab. C.2). Exceptions are observed in the experiment *pvar* with a slightly higher RMS of 0.18 and a 29.4% higher RMS of 0.22 in the experiment *qmin*. The RMS of TWP decreases in all experiments and reaches its lowest value with 4.40 $\mathrm{kg\ m}^{-2}$ in the run *vdiff*. In these experiments, the largest reduction of RMS could be achieved only in either the modeled variance or skewness. In a next step, these single experiments were combined to come closer to the observational data both concerning the variance and the skewness. Employing the settings of the experiment *rsk* resulting the lowest RMS as well as a better spatial pattern of skewness and the experiment *vedd* having the lowest RMS of variance in one run (*rsk+vedd*) together, the deviation of variance decreases further (Tab. C.4) and the spatial pattern of skewness is retained (figure not shown). This combination of modifications has no impact on RMS of the total cloud cover and a small one on the TWP whose RMS of 4.96 $\mathrm{kg\ m}^{-2}$ is even lower than the one in the control run.

In a further experiment (*rsk+vedd+pvar*) the ability to generate negative skewness (*pvar*) was added to the previous modifications of the model (*rsk+vedd*). However, the skewness exhibits almost only negative values in this run so that positive skewness has to be increased artificially. To estimate the proper amount of positive skewness which must be added, a couple of runs were carried out upscaling the shape-parameter q stepwise by up to a factor of 2. The best agreement of modeled skewness to the observational data is achieved by the choice of a factor of 1.2. The spatial

pattern of skewness of this run (*rsk+vedd+par+skew*) is now similar to the observational data and shows besides positive values also negative ones in the low latitudes (Fig. 2.6e). Consequently, the RMS of skewness decreases to 0.68 being the lowest value of all experiments and if only the region between $30°\mathrm{S}-30°\mathrm{N}$ is considered, the RMS decreases to 0.32. The RMS of the variance of 9.35 $\mathrm{kg}^2\ \mathrm{m}^{-4}$ is somewhat lower than in the experiment *vedd* and it is considerably lower than in the control run. The other two analyzed parameters, the total cloud cover and the TWP change differently in this experiment. Whereas the deviation of TWP with an RMS of 5.06 $\mathrm{kg\ m}^{-2}$ is even lower than in the run without modifications, the RMS of total cloud cover increases by 17.6% to 0.20. Moreover, the relative mean error of total cloud cover inverts from 1.6% to -4.7% in this run.

2.5. Summary and Conclusions

The subgrid-scale variability scheme for water vapor and cloud condensate applied in the ECHAM5 climate model was evaluated globally with high resolution satellite data. For this purpose model experiments with two different resolutions (T42L19 and T63L31) were carried out using a prescribed sea surfaces temperature and sea ice distributions of 2004. Model simulated total cloud cover, mean TWP as well as its variance and skewness were compared with parameters derived from MODIS and deviations of it were calculated where statistically significant at a 95% significance level.

The results show that the mean total cloud cover and the mean TWP are on average relatively well simulated. Indeed, a closer look into the spatial pattern of total cloud cover indicates an underestimation of clouds on the western sides of the continents, where commonly shallow marine boundary-layer clouds prevail. The underestimation of stratocumulus clouds in GCMs is a common problem and was also reported by Medeiros and Stevens (2011). The spatial deviations of TWP being quite similar to the one of the total cloud cover seem more caused by deficiencies of the hydrological cycle since the RMSs of the results from a simulation with the statistical PDF scheme and the another one with the relative humidity scheme are almost equal to each other. However, large deficiencies were revealed trough the evaluation for both variance and skewness of the PDF. Skewness of the TWP is strongly overestimated in the Tropics, and underestimated in the extratropical regions. The former is mainly caused by the model condition allowing for only positive skewness compared to the satellite data, which shows negative skewness in particular in the Tropics. Systematically negative deviations of variance are found for almost all regions of the globe. The above described patterns were found for both analyzed resolutions, where the coarser one exhibits a somewhat smaller RMS of TWP, a somewhat higher RMS of its skewness, and a considerably larger RMS of its variance. The RMSs of total cloud cover are almost equal in both resolutions as well as in the PDF scheme and in the relative humidity cloud scheme.

Moreover, some sensitivity experiments were made to analyze the parameterization of atmospheric processes affecting the variance and skewness, and to adjust the parameterization of these statistical quantities. The results indicate that the DW is increased by reducing the dissipation caused by vertical eddies, which has a stronger impact than the dissipation caused by horizontal eddies or the vertical diffusion of this quantity. Although the modeled variance was improved by these

adjustments, there is still a negative bias, which could possibly be caused by the precipitation process removing too much liquid water from clouds within one timestep. Additionally, the flawed skewness (shape-parameter q) coupled with the variance (distribution width) through its prognostic equation also contributes to the bias of modeled variance. However, the flawed variance also affects the skewness as demonstrated in the experiment in which the omitted dissipation of DW caused by vertical eddies increases the skewness. The large positive bias in skewness in the Tropics is reduced considerably when the skewness was calculated only for deep convection indicating deficiencies in the link to the convection parameterization in the scheme. In order to obtain a further reduction of the bias, it is necessary to allow for negative skewness in the model. This was tested using a relation between the two shape-parameters of the PDF suggested by Tompkins (2008). With this modified parameterization, the model is able to produce mean negative skewness mainly in the high and mid-latitudes, but again positive skewness in the Tropics. It is possible to exploit this modification in order to achieve improved results of variance and skewness together when the different adjustments of the parameterizations are combined: 1) allowing negative skewness, 2) calculating skewness increase only for detrainment from ice-containing deep convection, 3) generally increasing positive skewness (shape-parameter q) by 20% and 4) reducing the dissipation of DW caused by vertical eddies.

Although only MODIS data were selected featuring a high confidence, there are some regions in the data with bright surfaces, e.g. snow, ice and sand, where the uncertainty of the satellite data is higher. Additionally, the interpolation of missing water vapor data below clouds being a result of the measurement method of MODIS, has also to be taken into account analyzing the deviations of the MODIS data. Moreover, the vertical integration of modeled TWP making the data comparable to the satellite data introduces biases into the evaluation. First, the maximum overlap assumption for the PDF of the total water mixing ratio has to be named. Assuming maximum overlap results in maximum variance and skewness for the vertical integral of total water mixing ratio - a potential overestimation of the distribution moments compared to other overlap assumptions such as random overlap. However, even for this maximum overlap assumption it was found that variance is strongly underestimated by the model. For skewness, the absolute value might be overestimated due to the overlap assumption, but the qualitative results - e.g., not enough negative skewness - are not affected. Thus, for our main conclusions the maximum overlap assumption is good enough. However, in future investigations, more elaborate overlap assumptions should be considered, such as approaches using sub-columns allowing to apply arbitrary overlap assumptions (e.g., Räisänen et al., 2004; Pincus et al., 2005; 2006). A second issue is the vertical integration itself which emphasizes the lower troposphere, in particular the PBL, but does not allow to specifically investigate the free and upper troposphere. However, the vertical integral is the only data currently available for an evaluation of the PDF scheme at a global scale, so this study should be seen as a first step in the evaluation. It should be noted that simulation results and observational data are treated consistently.

This evaluation shows that there is still an urgent need for further improvements of the subgrid-scale variability scheme for water vapor and cloud condensate. In the sensitivity studies varying the choices in current parameterization, even ones which more substantially modify the scheme by e.g., allowing for negative skewness, did not achieve a full agreement with the observed PDFs

of TWP. Specifically, in the current scheme, vertical downdrafts, which transport dry air from the upper atmosphere in the planetary boundary layer and produce negative skewness, are not taken into account in the prognostic equation of skewness. However, negative skewness in the lower atmosphere can be seen in the satellite data and negatively skewed distributions of total water mixing ratio in stratocumulus clouds have also been found by Zhu and Zuidema (2009), who analyzed various cloud cases with large eddy simulations (LESs). Moreover, they revealed that the variance of moisture and temperature are equally important in controlling subgrid-scale clouds. Thus, the inclusion of the subgrid-scale variability of temperature which is currently neglected could improve the scheme as well. The next logical step would be to exploit the information of the subgrid-scale variability of cloud condensate provided by the scheme in the precipitation formation such as the autoconversion or the accretion process.

3. Incorporating the Sugbrid-Scale Variability of Clouds in the Autoconversion

3.1. Introduction

Low level clouds are important regulators in the climate system due to their cooling radiative effect (Chen and Cotton, 1987; Bretherton et al., 2004). The radiative properties of these so-called warm clouds (those containing no ice) are defined by the size distribution of their droplets and the horizontal and vertical distribution of cloud liquid water. A decisive physical process in warm clouds is the autoconversion (coagulation) of cloud droplets determining the precipitation formation, and consequently cloud liquid water and cloud cover. Moreover, the autoconversion is the initiating process which is requisite for the following precipitation generating processes such as accretion (collecting cloud droplets by raindrops) or self-collection of raindrops.

The stochastic collection of cloud droplets, i.e. the growth of cloud droplets by coalescence, can be considered in terms of a droplet of mass m falling through a cloud with particles of mass $\acute{m}$. The probabilistic and discrete feature of this process is accounted for by regarding the size distribution of cloud droplets $N(m,t)$, with N as the number of droplets per volume with mass m at time t. A change of N with respect to time is referred as the stochastic collection equation (Houze, 1993)

$$\frac{\partial N(m,t)}{\partial t} = \frac{1}{2}\int_0^m K(m-\acute{m},\acute{m})N(m-\acute{m},t)N(\acute{m},t)d\acute{m} - \int_0^\infty K(m,\acute{m})N(\acute{m},t)N(m,t)d\acute{m}, \tag{3.1}$$

with

$$K(m,\acute{m}) \equiv A_m \mid V(m) - V(\acute{m}) \mid \sum\nolimits_c (m,\acute{m}), \text{ where } A_m = \pi(R+\acute{R})^2.$$

The first term in Eq. (3.1) describes the rate of generation of droplets of mass m by coalescence of smaller droplets within the volume $d\acute{m}$. To prevent counting each collision twice, the factor of one half was included in the beginning of the equation. K is the collection kernel which determines the rate at which the space within which a particle of mass $\acute{m}$ is located is swept out by a particle of mass m. The second term expresses the rate of decrease of the number of droplets of mass m caused by their coalescence with droplets of mass $\acute{m}$ in the volume $d\acute{m}$. A_m denotes the geometrical cross-sectional area swept out by a particle of mass m which is assumed for water droplets as spherical with R and $\acute{R}$ as the radii of droplets of mass m and $\acute{m}$, respectively. V is the fall speed of the droplets of mass m and $\acute{m}$. The collection efficiency $\sum_c$ represents the efficiency

with which a droplet intercepts and collects the droplet it overtakes. It depends primarily by the relative airflow around the falling droplet and on the size of the droplet. However, it does not mean that each collision between two droplets leads to coalescence. They may also bounce off each other or will be divided after a short unification. The described stochastic collection process is commonly used as starting point to derive parameterizations for autoconversion and accretion.

Usually, two approaches are applied to simulate the autoconversion process in GCMs. One uses a threshold mean droplet radius above which autoconversion of cloud droplets occurs to account for the strong non-linearity of the coalescence. (Sundqvist, 1978; Boucher et al., 1995; Rotstayn, 1997). The other approach is a continuous parameterization coupling the cloud liquid water and the cloud droplet number concentration directly. This kind of parameterization can be derived from the stochastic collection equation describing the time evolution of a droplet spectrum (Beheng, 1994; Lohmann and Roeckner, 1996). Another parameterization for autoconversion in a large-eddy simulation (LES) was developed by Khairoutdinov and Kogan (2000) using a regression analysis of simulated drop sprectra. Although this formulation was derived only for the use in an LES, Posselt and Lohmann (2008) showed in their work that it is also applicable in a GCM.

The autoconversion as a local process takes place on a subgrid-scale, but it is parameterized by means of grib-box mean values. This introduces a bias since autoconversion is a non-linear process. Wood et al. (2002) found that the bias in the autoconversion rate caused by neglecting the subgrid-scale variability becomes larger the coarser the resolution of the model grid is. Furthermore, these biases become strengthened the larger the non-linearity is expressed, e.g. by the exponents in the equations (Pincus and Klein, 2000). Thus, the autoconversion process contributes to the uncertainty of modeled climate scenarios.

Several approaches were made to reduce the bias caused by neglecting the subgrid-scale variability of clouds, i.e. by tuning the critical threshold parameter at which autoconversion begins. Rotstayn (2000) was able to increase the critical threshold parameter to a more realistic value by restricting the occurrence of autoconversion only in the fraction of the cloudy area determined by a triangular PDF of total water mixing ratio. A direct incorporation of inhomogeneity within clouds in the continuous autoconversion parameterization derived by Beheng (1994) was made by Zhang and Lohmann (2002). They used a PDF of a Gaussian distribution to introduce the in-cloud variability of cloud liquid water in autoconversion process. The new scheme was implemented and tested in the Canadian Single Column Model and led to improvements in terms of liquid water path in three analyzed case studies.

Another approach to account for the subgrid-scale variability of cloud cover and microphysical properties in stratiform precipitation formation was done by Jess (2010). In this approach, each model column is divided into independent sub-columns with sub-boxes in each layer. Then, cloud cover is distributed depending on the diagnosed fraction and the maximum-random overlap assumption in the sub-boxes. A prescribed PDF determined by measurements from aircraft observations is applied to distribute cloud droplets and ice crystals over the cloudy sub-boxes. Simulations with the ECHAM5 climate model resulted an earlier onset of precipitation and better agreement with observations. A more complex description for a warm-rain microphysics parameterization taking into account the subgrid-scale variability was developed by Cheng and Xu (2009). For in-

stance, they derived an analytical expression for autoconversion by integrating an equation for the autoconversion rate over a joint-double Gaussian PDF of vertical velocity, liquid water potential temperature, total water mixing ratio and perturbation of rainwater mixing ratio for simulations in a single column model (SCM).

The tuning of autoconversion (Rotstayn, 2000) intends to obtain realistic accumulated precipitation in comparison to rain gauge networks or satellite retrievals. In coarse GCMs, this is achieved by too frequent precipitation of too low intensity. Nam (2010) found higher frequencies for low precipitation intensities in the ECHAM5 climate model compared to CloudSat satellite retrievals. A similar issue was reported from the HIRHAM regional climate model, whose convection scheme tends to artificially produce light precipitation (May, 2008). The described problems of modeled precipitation frequencies and intensities can be a result of neglecting the subgrid-scale variability of cloud condensate. Replacing the mean cloud liquid water in the precipitation parameterization by a simulated distribution of cloud liquid water for each model grid-box may reduces the afore-mentioned biases. This can be achieved by applying a PDF of total water mixing ratio emphasizing isolated areas of cloud liquid water (single clouds). Thus, an increase of occurrence of higher autoconversion rates and a decrease of lower ones are expected to obtain.

In this chapter, a revised continuous autoconversion parameterization for warm clouds in a GCM is presented which accounts for the subgrid-scale variability of cloud liquid water. The new parameterization combines the autoconversion derived by Beheng (1994) with the statistical PDF approach described by Tompkins (2002) using an integral of the autoconversion rate over the saturated part of the PDF. Furthermore, the new scheme is evaluated and compared with the original autoconversion parameterization using sensitivity simulations in the ECHAM5 climate model. In detail, the modified autoconversion rate and its impact on accretion, vertically integrated cloud liquid water, total cloud cover, cloud radiative forcing (CRF) as well as on the total and large-scale precipitation and their statistics are analyzed. In Section 3.2, the new autoconversion parameterization is introduced and compared with the original scheme. Section 3.3 discusses the theoretical aspects of the impact of negative skewness on the autoconversion rate. Subsequently, in Section 3.4, the different model experiments and methods as well as the observational data are described. The results of the model simulations are analyzed in Section 3.5, and a summary and outlook closes the chapter in Section 3.6.

3.2. Introducing the Subgrid-Scale Variability of Clouds

In the current version of the ECHAM5 climate model (Roeckner et al., 2003), the autoconversion rate Q_{aut} derived from the stochastic collection equation given by Beheng (1994) (in SI units) is applied

$$Q_{aut} = \alpha \left(\frac{\overline{r_l}}{C} \right)^{4.7} \tag{3.2}$$

with

$$\alpha = \gamma_1 \left(6 \cdot 10^{28} n^{-1.7} \left(10^{-6} N_l \right)^{-3.3} \left(10^{-3} \rho \right)^{4.7} \right) \frac{1}{\rho},$$

where γ_1 is a "tunable" parameter determining the efficiency of the autoconversion process, and hence, cloud lifetime; $n(= 10)$ is the width parameter of the initial cloud droplet spectrum, N_l the cloud droplet concentration, ρ the air density, $\overline{r_l}$ the grid-box mean cloud liquid water and C the cloud fraction in the model grid-box.

To incorporate the subgrid-scale variability of cloud liquid water into the autoconversion process, the PDF approach developed by Tompkins (2002) is used. The approach is already employed to incorporate the subgrid-scale variability of water vapor and cloud condensate in the cloud cover scheme in the model. The scheme uses a beta-function based PDF of total water mixing ratio to calculate the horizontal cloud fraction by an integral of the saturated part of a PDF (a description of the scheme can be found in Chapter 2). Following this statical approach, and assuming saturation within the cloud, the mean cloud liquid water $\overline{r_l}$ is written in warm clouds $(T > 0\ \mathrm{C}^\circ)$ as

$$\overline{r_l} = \int_{r_s}^{b} (r_t - r_s) G(r_t) dr_t. \tag{3.3}$$

Thus, the mean cloud liquid water $\overline{r_l}$ is equal to the integral over the difference of the total water mixing ratio r_t and the saturation vapor mixing ratio r_s, for the PDF of the beta-function G from the saturation vapor mixing ratio to the maximum of the total water mixing ratio subgrid-scale horizontal distribution b. G is defined as

$$G(r_t) = \frac{1}{B(p,q)} \frac{(r_t - a)^{p-1} (b - r_t)^{q-1}}{(b-a)^{p+q-1}}, \tag{3.4}$$

with

$$B(p,q) = \frac{\Gamma(p)\Gamma(q)}{\Gamma(p+q)}, \tag{3.5}$$

for $a \leq r_t \leq b$, $p > 0$, $q > 0$ and Γ as the gamma function, B the beta-function, a the minimum of the total water mixing ratio subgrid-scale horizontal distribution as well as p and q the shape-parameters of the beta-distribution. The constraint that Eq. (3.3) can be only applied for warm clouds is necessary to exclude the cloud ice from the cloud condensate, which is obtained by

the integral of the saturated part of the PDF. Replacing the cloud liquid water in Eq. (3.2) by Eq. (3.3), the subgrid-scale variability of cloud liquid water is introduced in the autoconversion process. Consequently, the in-cloud autoconversion rate turns to the mean value of a grid-box

$$\overline{Q}_{aut} = \alpha \int_{r_s}^{b} (r_t - r_s)^{4.7} G(r_t) dr_t. \tag{3.6}$$

To obtain the autoconversion rate inside the cloud, Eq. (3.6) has to be divided by the cloud fraction C of the respective grid-box:

$$Q_{aut} = \frac{\overline{Q}_{aut}}{C}. \tag{3.7}$$

The implementation of this revised autoconversion scheme into the existing cloud module of the model requires an additional algorithm for numerical integration of the integral in Eq. (3.6) and the time-integration of the autoconversion rate Eq. (3.2) which is described in Appendix A.

An overview of the theoretical distribution of the new autoconversion rates can be seen in Fig. 3.1a. It shows in-cloud autoconversion rates for different choices of q and r_s depicted as saturated part of the PDF. The DW is set to constant for this example (minimum of total water mixing ratio is set to 0.001 and its maximum to 0.01 $\mathrm{kg\ kg^{-1}}$). In-cloud liquid water content, and thus autoconversion increases with increasing saturated part of the PDF, and with decreasing skewness. The white area is caused by very low cloud fractions ($C < 0.001$) considered as clear sky in a grid-box and is equal to the clear sky area in the grid-box (Fig. 3.1b). It shows high cloud fraction in the red colored area starting from a symmetric and highly saturated PDF towards a skewed and completely saturated PDF of total water mixing ratio. The distribution of the amount of the new autoconversion rates resembles strongly the one of the amount of the in-cloud liquid water content in Fig. 3.1c. This makes sense because the autoconversion depends strongly on the amount of cloud liquid water being converted to raindrops.

For some considerations of the shape-parameter q and the saturated part of the PDF (respectively at some autoconversion rates) the entire liquid water is removed out of the cloud within one timestep. The area indicating this process for a given timestep of the applied model resolutions ($\Delta t = 1800\mathrm{s}$ for T42) is shaded in Fig. 3.1a. The area covers mostly moderate and high autoconversion rates starting with a symmetric and 15% saturated PDF towards a more skewed ($q \approx 34$) and saturated PDF.

To compare the new autoconversion rate with the original one, the ratio of both is determined (Fig. 3.1d). For this purpose, the original rate is calculated using the in-cloud liquid water of the PDF of total water mixing ratio divided by the respective cloud fraction for each q and r_s. The comparison of the new and the original autoconversion rate shows fundamental differences concerning the amount. In all configurations of skewness and saturated part of the PDF, the new rate is higher, actually in some cases considerably higher, than the original one. In detail, the ratio increases up to 55 when the PDF becomes saturated and skewed, but the ratio decreases strongly when the PDF is entirely saturated, or when the PDF becomes symmetric. A main result is therefore that the new autoconversion scheme produces higher rates in general, but clearly higher autoconversion rates in partly skewed-PDF conditions compared to the original one.

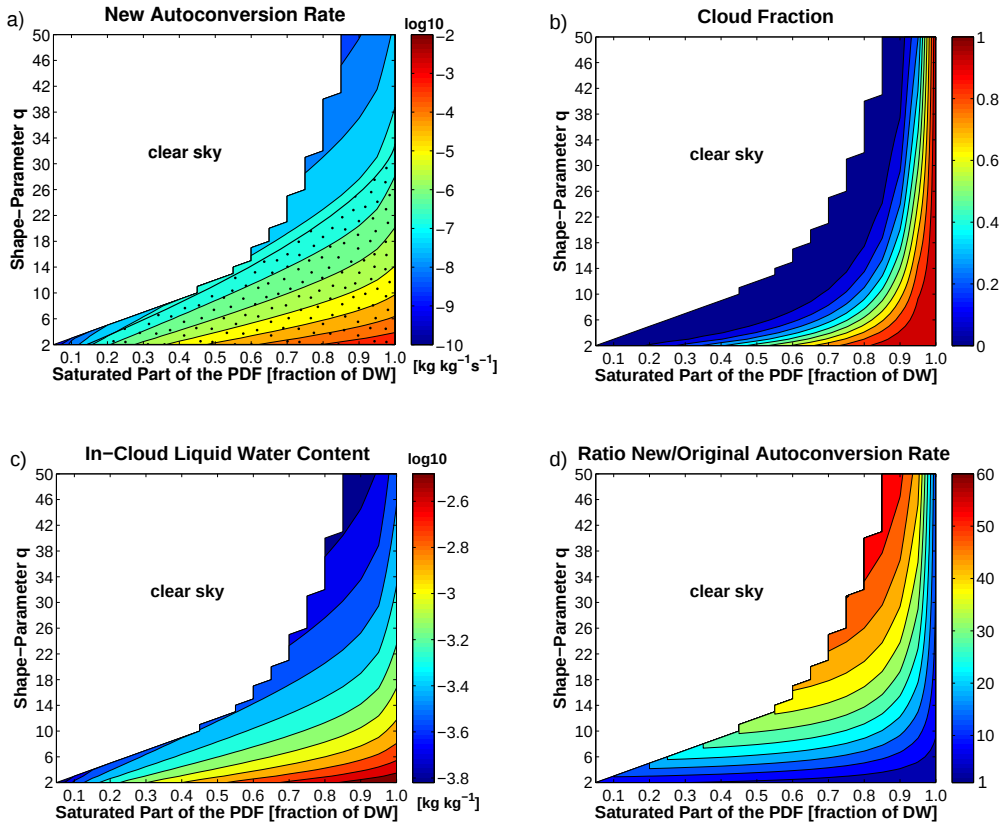

Figure 3.1.: Dependency of the new autoconversion rate (a), cloud fraction (b), in-cloud liquid water content (c) and the ratio of the new and the original autoconversion rate (d) on the shape-parameter q and the saturation vapor mixing ratio depicted as saturated part of the PDF. The distribution width (DW) is set to constant for simplifications (minimum of total water mixing ratio is set to 0.001 and its maximum to 0.01 kg kg^{-1}) and the dotted area in (a) indicates the rates at which the whole cloud liquid water is removed out of the cloud within one timestep for T42 ($\Delta t = 1800$s).

3.3. Impact of Negative Skewness on Autoconversion

The statistical cloud cover scheme uses a beta-function based PDF to describe the distribution of total water mixing ratio within a grid-box. The shape of the PDF is flexible and determined by the two shape-parameters p and q (see Fig. 3.2) as well as a and b, which change according to atmospheric processes, e.g. precipitation and turbulence on the PDF. A PDF of total water mixing ratio exhibits positive skewness ($q > p$, red curves in Fig. 3.2) when low values of total water mixing ratio are more likely than high values in a grid-box and has typically a tail on its right side towards higher total water mixing ratio values. This simulates, depending on the saturation vapor mixing ratio, the presence of a few thick clouds caused e.g. by vertically transported moisture (updrafts and detrainment). A negatively skewed PDF of total water mixing ratio ($q < p$, blue

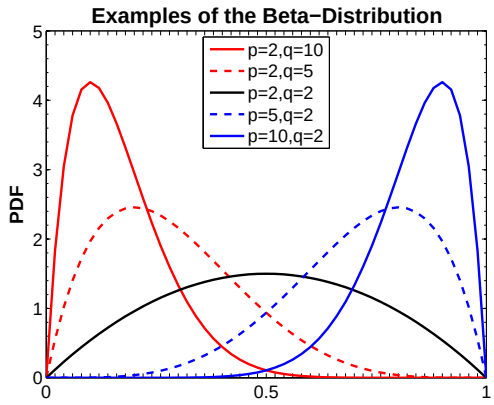

Figure 3.2.: Various beta-distributions which depend on different combinations of the shape-parameters p and q. Red curves indicate positively skewed distributions, blue negatively skewed distributions and black a symmetric one.

curves in Fig. 3.2) represents the opposite situation when high values of total water mixing ratio are more likely than low values in a grid-box and the PDF has a tail on its left side towards lower total water mixing ratio values. In this case, the grid-box exhibits, depending on the saturation vapor mixing ratio, more clouds than areas with dry air, i.e. without clouds. These areas can be caused e.g. by downdrafts transporting dry air from the upper to the lower atmosphere.

In the current version of the statistical cloud cover scheme, which provides the information for the new autoconversion scheme, only positive or zero skewness is allowed due to simplifications of the prognostic equations. However, the evaluation of the statistical cloud cover scheme (Chapter 2) revealed that the modeled skewness is overestimated over the oceans, especially in the Tropics, compared with observational data, which shows also negative skewness. To adjust the modeled skewness of the cloud cover scheme closer to the observational data, it could be reasonable to introduce also negative skewness into the scheme. One attempt was made by Tompkins (2008) who proposed to let the shape-parameter p vary through the relation $p = (q + 1)/(q - 1)$ without introducing additional prognostic equations into the scheme. The distribution of the new autoconversion rates applying this parameterization as well as the ratio of the new and the original rate can be seen in Fig. 3.3a. Low liquid water content, and corresponding autoconversion rates occur in combination of either a symmetric and less saturated PDF or highly skewed and highly saturated PDF of total water mixing ratio. High rates are produced by almost a symmetric and highly saturated PDF. A direct comparison of the distributions of the new autoconversion parameterization allowing only positive skewness and the approach allowing also negative skewness (Figs. 3.1a/3.3a) is not practicable since the cloud liquid water determined by the PDF is different in these two parameterizations. Large differences to the original autoconversion rate calculated with this approach (allowing negative skewness) are observed for highly skewed and less saturated PDF indicated by ratios up to 60 (Fig. 3.3b).

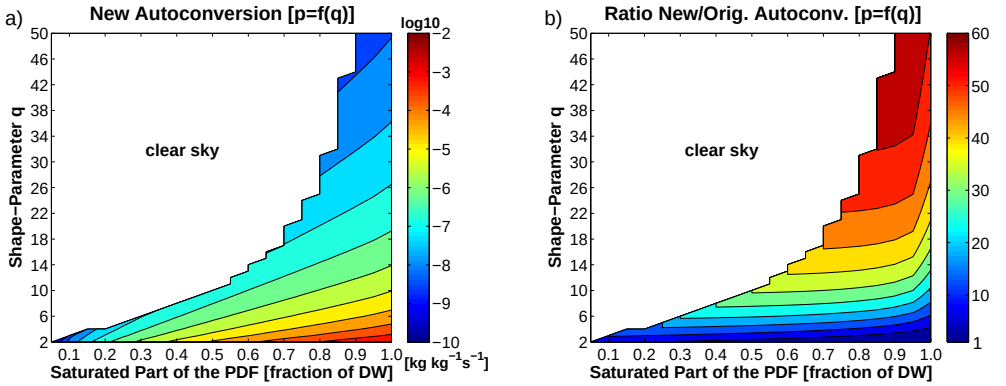

Figure 3.3.: Distributions of new autoconversion rates (a) and ratio of the new and the original autoconversion rate (b) using the approach $p = (q + 1)/(q - 1)$. The DW is set to constant for simplifications (minimum of total water mixing ratio is set to 0.001 and its maximum to 0.01 kg kg^{-1})

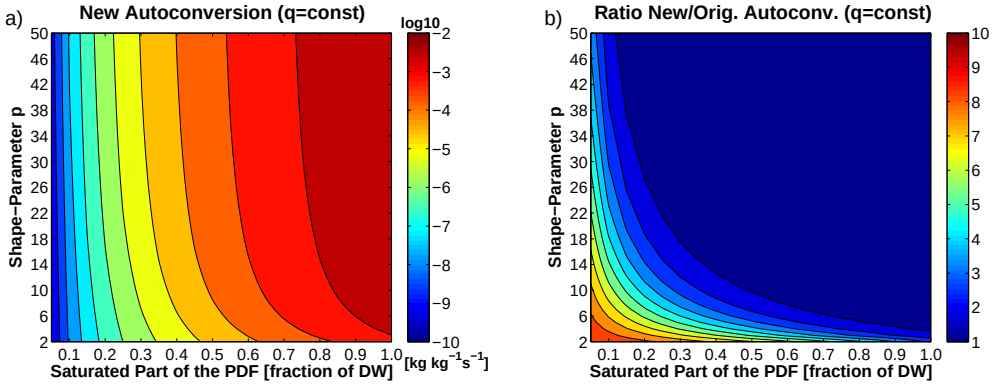

Figure 3.4.: Distributions of new autoconversion rates (a) and ratio of the new and the original autoconversion rate (b) fixing the shape-parameter q and varying p. The DW is set to constant for simplifications (minimum of total water mixing ratio is set to 0.001 and its maximum to 0.01 kg kg^{-1})

A broader range of high autoconversion rates is obtained when only a symmetric or negatively skewed PDF of total water mixing ratio is allowed in the parameterization fixing shape-parameter q and varying p (Fig. 3.4a). In this case, high liquid water content and corresponding high rates occur in combination of a strongly negatively skewed and an already moderately saturated PDF, whereas low ones are only produced when the PDF of total water mixing ratio is low saturated. A comparison with the original autoconversion rate shows that the new autoconversion parameterization allowing only symmetric or negatively skewed PDFs is higher in all combinations of p and r_s (Fig. 3.4b). In particular, this is found for close-to symmetric and low saturated PDFs causing ratios up to the factor of 8. Altogether, allowing negative skewness in the statistical cloud cover scheme leads to a broader range of high autoconversion rates and decreases the range of low rates.

3.4. Methods and Observational Data

3.4.1. Model Experiments

The new autoconversion scheme was implemented in the cloud microphysics of the ECHAM5 climate model (Roeckner et al., 2003) to analyze the impact of the subgrid-scale variability of cloud liquid water in the autoconversion parameterization derived by Beheng (1994). For this purpose, a one year simulation with an hourly output interval was carried out with the ECHAM5 model starting three months earlier to reach an equilibrium for the cloud microphysical processes. Six different model experiments were made using a horizontal resolution at the equator of about 313 km (model grid T42) and a vertical resolution of 19 levels with the uppermost level at 10 hPa. The observed monthly mean sea surface temperature and sea ice data of 2004 were used as boundary conditions for the model experiments as in AMIP (Gates et al., 1999).

In the control experiment, the original autoconversion parameterization derived by Beheng (1994) was used as in standard ECHAM5 climate model. The new autoconversion parameterization was applied with two different values of the autoconversion tuning parameter γ_1 in Eq. (3.2). In an untuned experiment (standard version of the new parameterization), γ_1 was set equal to 15 as in the standard ECHAM5 configuration and, in a tuned one ($cr2$), equal to 2 which results in a balance of the net radiation (sum of SW and LW fluxes) at the top of the atmosphere (TOA).

Moreover, two additional experiments were carried out to analyze the sensitivity of the untuned autoconversion scheme to changes in the parameterization of DW and skewness (shape-parameter q) of the PDF employing the results from the evaluation of the statistically cloud cover scheme (Tompkins, 2002) in Chapter 2. In the first experiment labeled $vedd$, the DW was increased reducing the dissipation of the DW caused by vertical eddies by the factor of 10. In the second experiment $nqx2$, the parameterization of the cloud cover scheme is used which was found to provide the closest results to observational data concerning the DW and skewness (Chapter 2). This can be achieved by increasing the DW (as in the experiment $vedd$), applying skewness increasing from convective detraiment only for deep convection and allowing for negative skewness through the relation $p = (q+1)/(q-1)$ as suggested by Tompkins (2008) as well as an artificially increased shape-parameter q by 20%. In a further experiment labeled kk scheme, the autoconversion parameterization derived by Beheng (1994) was replaced by the parameterization $Q_{aut} = 1350(\overline{r_l}/C)^{2.47}N^{-1.79}$ developed by Khairoutdinov and Kogan (2000) in order to test whether the observed impact of the incorporated subgrid-scale variability of clouds is restricted to the original autoconversion parameterization.

3.4.2. Observational Data

The modeled quantities affected by the modified autoconversion parameterization are compared to ones in the control experiment, but also to various observational data measured by satellite and ground based instruments to assess the achieved improvements by the new scheme.

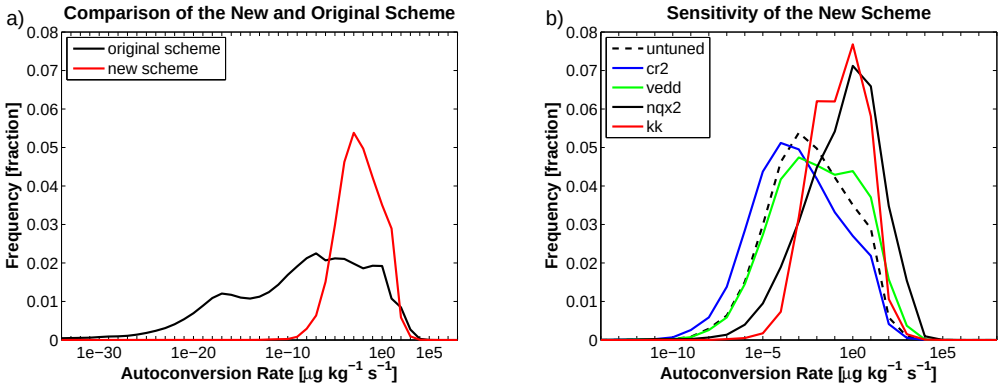

Figure 3.5.: Distribution of autoconversion rates calculated by the new and original scheme (a) and by different parameterizations of the sensitivity experiments (b) from all levels of one year.

Total cloud cover derived from the L2 Joint Product of MODIS on the Terra satellite (Platnick et al., 2003; King et al., 2003) was employed for the year 2004. The high spatial resolution (5×5 km^2) of the data helps to capture horizontal spatial subgrid-scale variability of total cloud cover. To compare the vertically integrated cloud liquid water simulated by the model, the column liquid cloud water (LWP) from MODIS (Liquid Water Cloud Water Path: Level-2 QA Weighted Mean) is used with a horizontal resolution of 1° degree grid-cells. LW and SW radiative fluxes were taken from the EBAF product of CERES (Loeb et al., 2008) which consists of 1° gridded five year averages of the TOA LW and SW radiative fluxes under clear- and all-sky conditions.

Two different datasets were used to verify the modeled total precipitation (sum of large-scale and convective precipitation). First, the HOAPS dataset which provides two times daily precipitation over the ocean for the year 2004 (Andersson et al., 2007, 2010) and, second, the GPCP dataset which incorporates satellite microwave and infrared data as well as surface rain gauge observations to estimate daily precipitation both over land and ocean (Adler et al., 2003; Huffman et al., 2009). For this evaluation, the product version 2.1 is employed providing precipitation at 1° horizontal resolution for the year 2004.

3.5. Results

3.5.1. Autoconversion Rate

A comparison of the new and the original autoconversion parameterization reveals considerable differences in the mean autoconversion rates (Tab. C.5), in the range of the autoconversion rates and the distribution of their frequencies (Fig. 3.5a). The mean autoconversion rate (averaged over all cloudy grid-boxes of the entire 3D model domain for one year at hourly intervals) in the new scheme is 53.7% lower than the one in the original scheme with 53.1 μg kg^{-1} s^{-1}. However,

in detail, the new autoconversion scheme produces less small rates (below 1e-6 μg kg^{-1} s^{-1}) and notably more higher rates (between 1e-6 and 100 μg kg^{-1} s^{-1}) than the original one. Only autoconversion rates higher than 100 μg kg^{-1} s^{-1} are slightly more often generated by the original scheme, which is expressed in the mean value. In general, this result seems reliable, because the introduction of subgrid-scale variability of cloud liquid water should reduce the frequency and increase the amount of autoconversion compared to the use of the grid-box mean values.

However, the result does not totally agree with the comparison of new and original autoconversion rate calculated with same PDF integrated cloud liquid water and cloud fraction in Section 3.2, where the new autoconversion is always higher than the original one. The reason for that could be a feedback of the increased frequencies in the higher autoconversion rates producing lower cloud liquid water.

The impact of modified parameterizations of the new scheme can be seen in the mean values (Tab. C.5) and frequency distributions (Fig. 3.5b). In the tuned version of the scheme ($cr2$), the mean autoconversion rate is 72.9% lower than in the original scheme due to the decreased tuning factor from 15 to 2 in the autoconversion Eq. (3.2). Accordingly, its frequency distribution is shifted to lower autoconversion rates and the maximum is somewhat lower compared to untuned version. An increase in the modeled DW of the total water PDF leads to an increase of the mean autoconversion rate in the experiment $vedd$ and, therefore to a reduction of the deviation to -18.3% related to the original scheme. This corresponds to a shift of the right side of the frequency distribution towards higher values. A further increased mean autoconversion rate being 272.7% over the one in the original scheme is resulted by a shift of the entire frequency distribution towards higher values in the experiment $nqx2$. This can be reasoned with increased DW of the total water PDF and the allowed negative skewness as explained in Section 3.3. The kk scheme produces a mean autoconversion rate which is 14.5% lower related to original scheme, and the smallest and highest frequency distribution of all experiments.

3.5.2. Accretion Rate

The autoconversion process in the model affects also the accretion process which can be seen in Tab. C.5 and Fig. 3.6a. In the microphysics scheme in the model, the accretion rate Q_{racl} is parameterized in two terms (Beheng, 1994):

$$Q_{racl} = \min(C, C_{pr}) d_1 \left(\frac{\overline{r_l}}{C} \right) \rho r_{rain} + \gamma_2 \rho Q_{aut} \Delta t, \tag{3.8}$$

with $d_1 = 6$ m^3 kg^{-1}s^{-1}, $\overline{r_l}/C$ as in-cloud liquid water, ρ as air density and γ_2 as "tunable" parameter. The first term simulates the falling mass mixing ratio of rain r_{rain} into the covered part C_{pr} of the grid-box and the second one the rain production during the timestep Δt by autoconversion. Consequently, the accretion rate contains the autoconversion rate directly, but it is also included by the generated raindrops and the decreased cloud liquid water, indirectly.

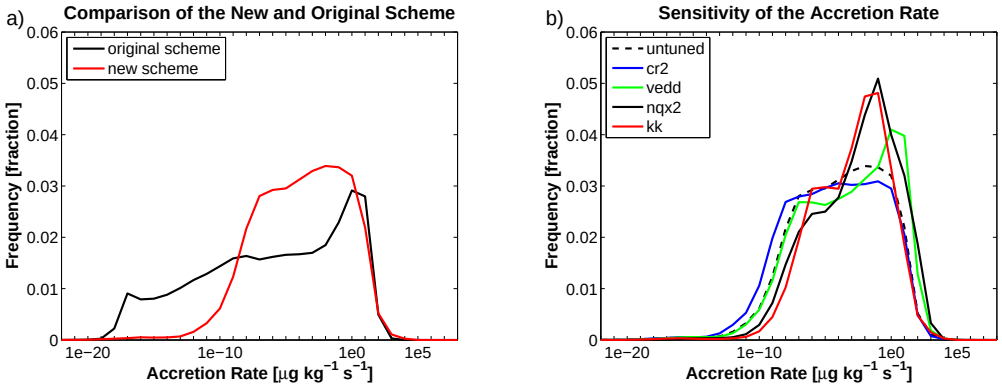

Figure 3.6.: Distribution of accretion rates affected by the new and original autoconversion scheme (a) and by different parameterizations of the sensitivity experiments (b) from all levels of one year.

The mean accretion rate (averaged over all cloudy grid-boxes of the entire 3D model domain for one year at hourly intervals) is increased by 237.3% using the new autoconversion scheme compared to the original scheme. The maximum of the frequency distribution of the accretion is slightly shifted to lower rates, but the maximum is more pronounced and covers the broader range of values (also to higher values). Moreover, a reduction of the occurrence of low rates occur applying the new autoconversion scheme. These findings can be explained by the increased occurrence of high autoconversion rates represented in the second term of Eq. (3.8). The fact that the tuned experiment ($cr2$) shows a quite similar distribution of accretion rates (Fig.3.6b) with higher mean cloud liquid water (see Section 3.5.3) implies that the collection process of cloud droplets by falling raindrops plays only a secondary role. Thus, the second term of the accretion parameterization leads to the observed distribution of accretion rates in general.

Changes in the mean rate and the frequency distribution of the accretion rate can also be seen in the modified parameterizations of the new autoconversion scheme (Fig. 3.6b). The maximum frequency of accretion rates in the tuned version of the scheme ($cr2$) is somewhat lower and the left side of its distribution tends towards lower rates compared to the untuned one. As a result, the mean rate is only 129.3% higher than the one in the original scheme. In the experiment $vedd$, the right side of the frequency distribution is shifted towards higher rates as well as its maximum being also higher than the untuned version. Hence, the mean accretion rate increases as well and is 371.7% above the original one. Similar changes in the mean rates and the frequency distributions can be observed in the kk scheme and the experiment $nqx2$. Whereas the kk scheme exhibits a higher frequency maximum than the untuned version and only the left side of the frequency distribution is shifted towards higher rates, the experiment $nqx2$ shows the highest frequency maximum and the entire distribution shifted towards higher accretion rates. Both experiments, $nqx2$ and the kk scheme, simulate higher mean rates with 463.6% and 362.6% above the mean of the original scheme.

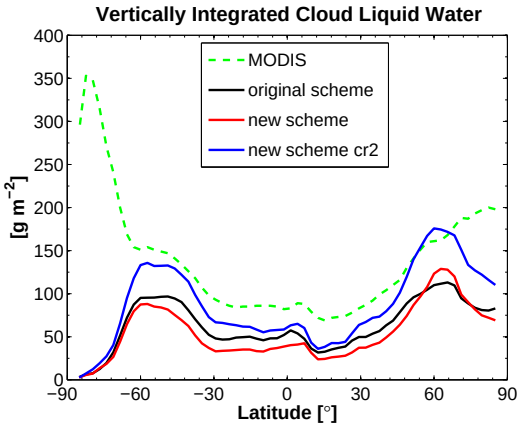

Figure 3.7.: Comparision between the zonal annual mean of vertically integrated cloud liquid water simulated by the original autoconversion, and the untuned ("new scheme") and tuned ("new scheme $cr2$") version of the new autoconversion scheme as well as the column liquid cloud water derived from MODIS.

3.5.3. Cloud Liquid Water

A modification of the autoconversion process in the model has a direct impact on the bulk of cloud liquid water, but also the accretion process modified again by the autoconversion of cloud droplets affects the cloud liquid water as explained in the Section 3.5.2 before. Increasing the cloud liquid water turnover in both processes decreases the liquid cloud water, but the autoconversion is generally more important one since it initiates the precipitation process in warm clouds. Furthermore, it has to be mentioned that the precipitation generation in convective clouds (including also mixed-phase and ice clouds) has also a small impact on the cloud liquid water.

In the experiment using the untuned version of the new autoconversion scheme, the mean vertically integrated cloud liquid water is 18% lower than the one applying the original scheme with 61 g m^{-2}. This seems curious since the mean autoconversion rate is also decreased in this experiment. However, at the same time, the mean accretion rate is increased by 230% overcompensating the reduction in the autoconversion. A different result is obtained when the autoconversion is further decreased as in the tuned experiment ($cr2$). In this one, the mean vertically integrated cloud liquid water is increased by 34.4%, whereas the mean accretion rate is lower than in the untuned one and increased only by 130% compared to the control experiment. This implies that at a certain amount of autoconversion, the accretion process does not (over)compensate the reduction of the autoconversion anymore.

The zonal mean distribution of the vertically integrated cloud liquid water simulated by the new autoconversion scheme is always lower than the one by the original scheme, except for the region around 60°N where the new scheme retains more cloud liquid water in the atmosphere (Fig. 3.7). A general increase of cloud liquid water in all regions can be observed in the tuned experiment, which gives a better fit to the MODIS derived column liquid cloud water compared to the original

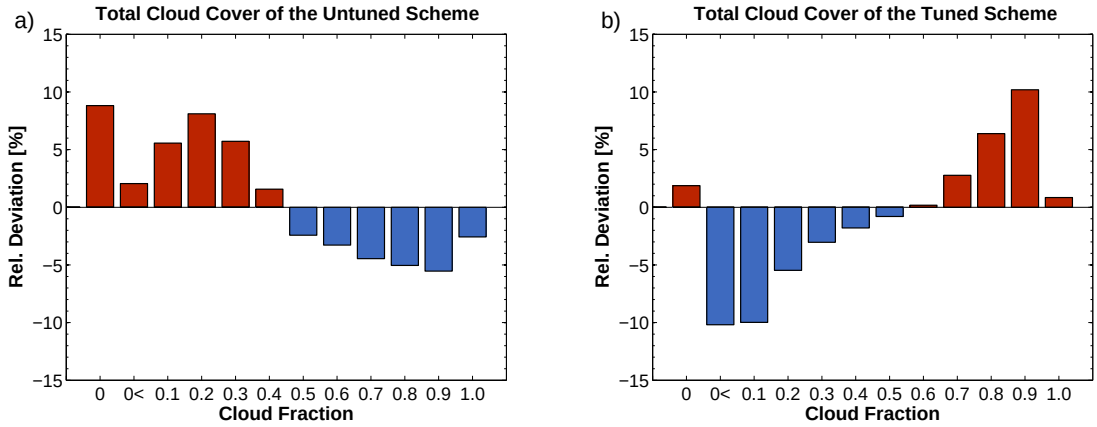

Figure 3.8.: Deviation of total cloud fraction in the untuned (a) and tuned (b) experiment from the control experiment. Grid-boxes having clear sky or being overcast are assigned to the bins labeled zero or one, respectively. Other bins have equal bin width containing grid-boxes with cloud fraction larger equal to the labeled bin, except for the bin labeled as larger than zero.

scheme. The unrealistically high LWP in the polar regions shown in the observational data seems more a result of the specific measurement methods of MODIS and were reported by Seethala and Horváth (2010). However, the tuned new autoconversion scheme overestimates the cloud liquid water somewhat around 60°N. The fact, that both untuned and the tuned version of the new scheme show higher values of cloud liquid water around 60°N than in the control experiment might indicate deficiencies in the parameterization of the simulated PDF of total water mixing ratio over land.

3.5.4. Total Cloud Cover

Cloud cover is determined by the presence of cloud condensate consisting of liquid cloud droplets and cloud ice. Therefore, the cloud cover is influenced by the autoconversion process (but also by accretion) through removing liquid cloud droplets, as can be seen in the total cloud cover (Tab. C.5). The untuned version of the new autoconversion scheme decreases the total cloud cover by 3.8% related to 0.63 cloud cover in the control experiment corresponding to the decreased cloud liquid water (see Section 3.5.3). The opposite effect can be observed when the tuned scheme ($cr2$) is applied. In this experiment, the total cloud cover increases by 1.6% which is due to higher amount of the cloud liquid water in the atmosphere. However, the increase of cloud cover is much lower than the increase of cloud liquid water compared to the case when the cloud cover is decreased by the untuned scheme.

A deviation of total cloud fraction related to the original scheme is observed as well. The untuned scheme simulates about 9% more cloud free grid-boxes and about 2.5% less grid-boxes being

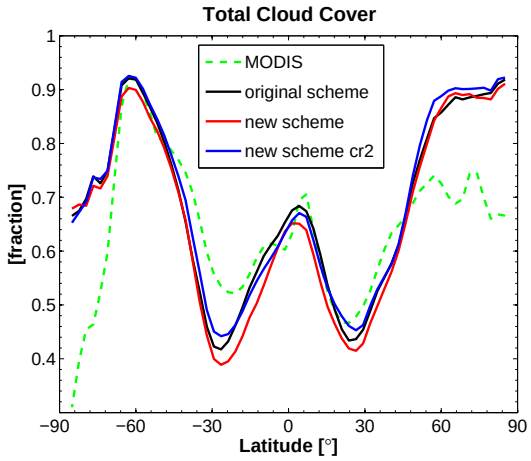

Figure 3.9.: Comparison between the zonal annual mean total cloud cover simulated by ECHAM5 with the original autoconversion as well as the untuned ("new scheme") and tuned ("new scheme $cr2$") version of the new autoconversion scheme, and the cloud cover derived from MODIS.

overcast (Fig. 3.8a). Furthermore, the number of grid-boxes having lower than 0.5 cloud fraction increases, whereas the number of them equal to or higher than 0.5 decreases. However, this reverses in the tuned experiment ($cr2$), where number of the grid-boxes having lower than 0.6 cloud fraction decreases and the one higher or equal to this threshold increases (Fig. 3.8b). This effect may be a result of the shift of autoconversion rates to lower values as well as more lower accretion rates in the tuned experiment, in which smaller amounts of cloud liquid water are removed within one timestep from the cloud leaving more of cloud liquid water.

The zonal mean distributions of total cloud cover affected by the original autoconversion scheme, the untuned and tuned version of the new scheme as well as the cloud cover derived from MODIS are depicted in Fig. 3.9. The untuned autoconversion scheme leads to a slightly lower total cloud cover in all regions except around $60°$N compared to the control experiment. Somewhat lower total cloud cover is also simulated by the use of the tuned scheme in the inner Tropics and higher one between $45°$S$-25°$S and $25°$N as well as from $45°$N towards the North Pole. Equal amount of total cloud cover are modeled around 60°S in the tuned and the control experiment. The overestimation of total cloud cover from $45°$N towards the North Pole and underestimation around $30°$S of all model experiments (including the original scheme) are probably caused by deficiencies in the cloud cover scheme (see Chapter 2). Improvements compared to the MODIS derived cloud cover are achieved between $45°$S$-25°$S and $25°$N using the tuned autoconversion scheme.

The western parts of the continents are of special interest since low level clouds (stratocumulus clouds) prevail in these regions and commonly, the GCMs are not able to simulate these clouds properly (Medeiros and Stevens, 2011). A direct comparison between the tuned version of the new scheme and the original autoconversion scheme reveals a further reduction of total cloud cover in those regions (Fig. 3.10). Consequently, no improvements are achieved when the tuned autoconversion scheme is applied because the cloud cover is already underestimated in those regions by the standard configuration.

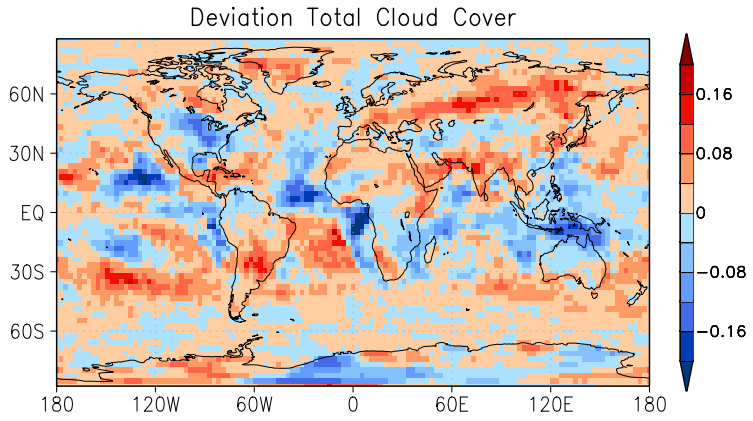

Figure 3.10.: Deviation of total cloud cover simulated in the tuned experiment from one using the original autoconversion scheme.

3.5.5. Cloud Radiative Forcing

The difference between the radiation budget for all-sky conditions and cloud-free conditions is labeled as CRF with respect to the net solar (shortwave) and the emitted terrestrial (longwave) radiation. As shown in the previous section, the modified autoconversion parameterization changes the total cloud cover, and affects therefore also the CRF.

Applying the untuned version of the new scheme, the mean SW CRF is decreased by 13%, whereas the tuned version ($cr2$) increases the forcing by 1.5% relative to the one in the control experiment with -49.3 Wm^{-2} (Tab. C.5). These results can be explained with the decreased, and slightly increased mean total cloud cover in the respective experiments (see Section 3.5.4). However, the changes of the CRF are regionally different in both parameterizations of the new scheme (Fig. 3.11a). Compared to the old autoconversion experiment, the SW CRF is in some parts considerably lower (up to -11.5 Wm^{-2}) between $60°\mathrm{S}-60°\mathrm{N}$ in the untuned experiment, and higher between $60°\mathrm{S}-25°\mathrm{S}$ and $50°\mathrm{N}-65°\mathrm{N}$ in the tuned one. Moreover, lower forcing is observed in the inner Tropics ($15°\mathrm{S}-15°\mathrm{N}$) when the tuned version of the new scheme is used. In general, a systematically better simulation of SW CRF related to the CERES EBAF measurements is not achieved applying both the untuned and tuned version of the new autoconversion scheme.

Smaller changes in the LW CRF are caused by the new autoconversion scheme. The untuned version of the new scheme decreases the mean forcing by 0.8%, whereas the tuned one increases it by 1.4% relative to the control experiment. As for the SW CRF, these results can be explained by the change in total cloud cover. Regional differences in the LW CRF of the experiments are depicted in Fig. 3.11b. The untuned version of the scheme leads to lower forcing around $60°\mathrm{S}$, $15°\mathrm{S}$, $10°\mathrm{N}$ as well as between $35°\mathrm{N}-60°\mathrm{N}$ and higher around $5°\mathrm{S}$ compared to the control experiment. Furthermore, higher LW CRF is simulated in the tuned experiment around $30°\mathrm{S/N}$ and $60°\mathrm{S/N}$. Slight improvements related to the CERES EBAF measurements are achieved around $60°\mathrm{S}$ and $10°\mathrm{S}$ by the untuned and around $30°\mathrm{S/N}$ by the tuned version of the the new scheme.

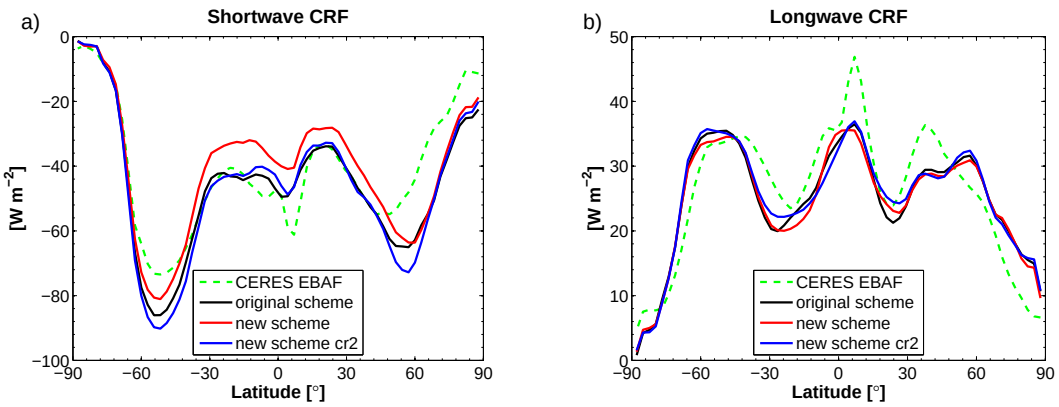

Figure 3.11.: Comparison between the zonal annual mean CRF for SW (a) and LW (b) spectra simulated by ECHAM5 with the original autoconversion as well as the untuned ("new scheme") and tuned ("new scheme $cr2$") version of the new autoconversion scheme, and the CRF derived from CERES EBAF satellite observations.

3.5.6. Large-Scale Precipitation

The autoconversion of cloud droplets to raindrops in warm ($T > 0°\mathrm{C}$) and mixed phased clouds ($-35°\mathrm{C} \leq T < 0°\mathrm{C}$) is the crucial process for generating large-scale precipitation. On the one hand, it produces raindrops being the prerequisite for the accretion process (collection of cloud droplets by falling rain) and, on the other hand, it decreases directly the amount of cloud liquid water. The autoconversion also indirectly affects the accretional growth of falling snow by collecting cloud droplets. This microphysical process contributes also to the large-scale precipitation.

The untuned version of the new autoconversion parameterization simulates almost the same mean large-scale precipitation rate P as the original one with $0.047\ \mathrm{mm\ h^{-1}}$, whereas the tuned version ($cr2$) causes a small reduction by -2.1%. Actually, the mean precipitation rate in the untuned experiment is slightly lower by $0.0005\ \mathrm{mm\ h^{-1}}$, but it can be seen due to the rounding effect. To analyze the changes in large-scale precipitation rates in the model domain, the rates are roughly classified in five categories which are explained exemplarily at the hand of the control experiment on a global scale (Fig. 3.12a). The first category contains the grid-boxes having rates larger than zero and smaller than $0.001\ \mathrm{mm\ h^{-1}}$. Its high percentage of 49.6% is a result of fact that ECHAM5 produces artificially very small precipitation rates down to $10^{-15}\ \mathrm{mm\ h^{-1}}$ all the time in hourly model output (which means that there is almost no grid-box where the precipitation rate is exactly zero). A similar problem is observed in simulations of the HIRHAM regional climate model, whose convection scheme tends to artificially produce light precipitation (May, 2008). The second category with 15.4% contains grid-boxes having precipitation rates between $0.001 \leq P < 0.01\ \mathrm{mm\ h^{-1}}$ being below the value of $0.01\ \mathrm{mm\ h^{-1}}$ at which precipitation is considered as measurable (Glickman, 2000). Although both categories contribute only 0.1% and 1.1%, respectively, to the total amount of precipitation per year (Fig. 3.12b), they are investigated here in order to asses these artificially-produced very low precipitation rates in the model. Low precipitation rates considered as $0.01 \leq P < 0.1\ \mathrm{mm\ h^{-1}}$ have an occurrence of 24.5% and a

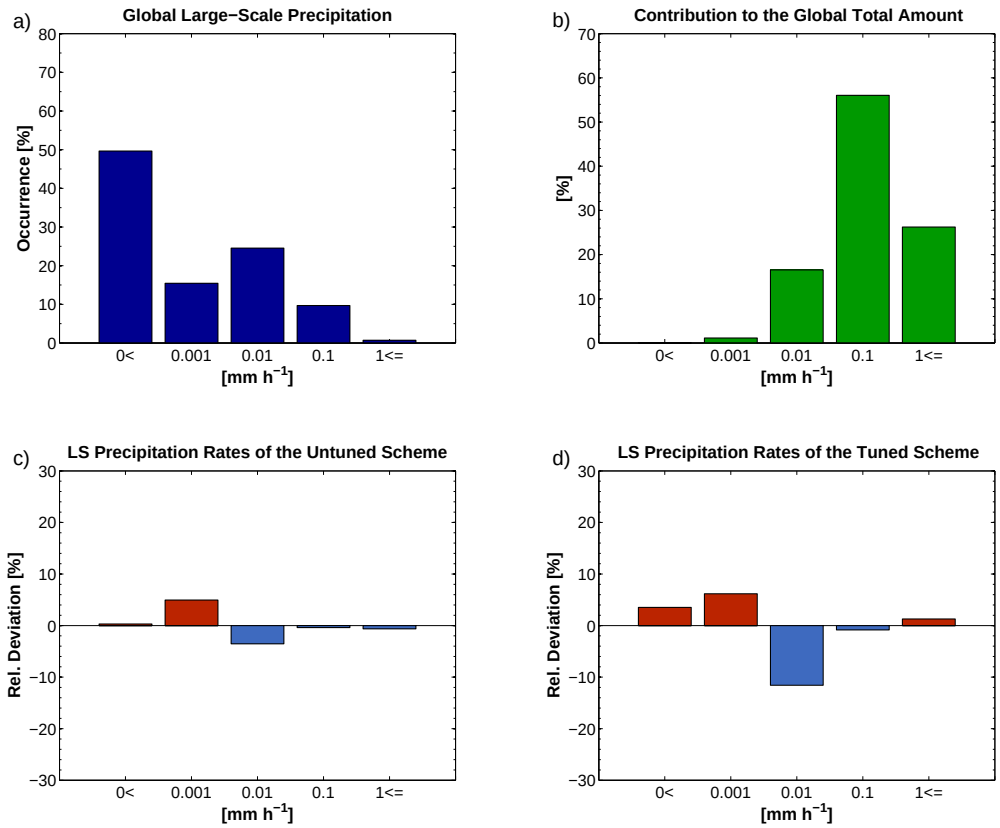

Figure 3.12.: Global large-scale precipitation: (a) occurrence of precipitation rates by categories in the control experiment [%], (b) contribution of categories to the total amount [%] and deviation of occurence [%] in the untuned (c) and tuned (d) experiment from the control experiment.

contribution to total accumulated precipitation of 16.5% in the model. Vali et al. (1998) were able to measure precipitation rates as small as $0.01\ \mathrm{mm\ h^{-1}}$ at the cloud base derived from radar instruments mounted on an aircraft. They label such low precipitation rates drizzle. Moderate precipitation rates classified by $0.1 \leq P < 1.0\ \mathrm{mm\ h^{-1}}$ contribute the most of all categories to accumulated precipitation with 56%, but have only a frequency of 9.7%. The lowest occurrence with 0.7% and a contribution of 26.2% to total precipitation has the category labeled as high precipitation rates containing grid-boxes with rates higher than $1.0\ \mathrm{mm\ h^{-1}}$.

Applying the new autoconversion scheme, low precipitation rates are decreased moderately by -3.5% in the untuned experiment and considerably, by -11.6%, in the tuned one (Fig. 3.12c/d). In both experiments, an increase of the artificially produced and non-measurable precipitation (categories one and two) is observed. The stronger increase in the tuned experiment may be the result of more cloud liquid water in the atmosphere (see Section 3.5.3). Furthermore, in the tuned experiment, the frequency of occurrence of high precipitation rates is increased by 1.3% in comparison to the control experiment. The reduction of low precipitation rates and the increase

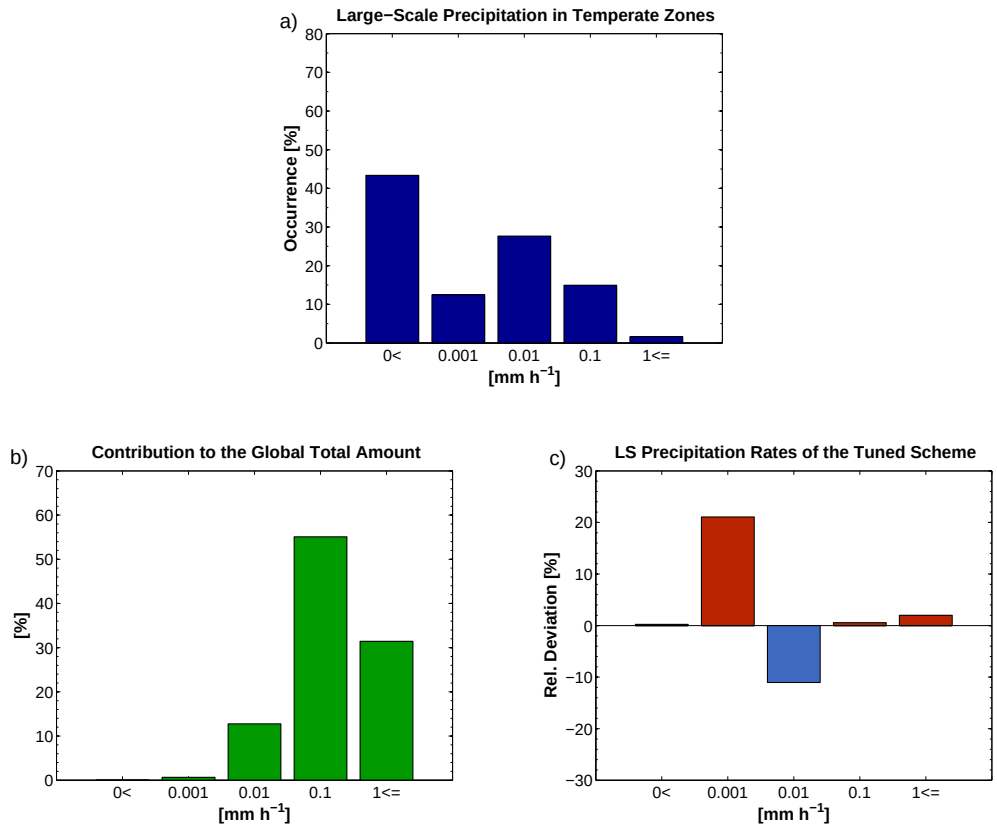

Figure 3.13.: Large-scale precipitation in temperate zones: (a) occurrence of precipitation rates by categories in the control experiment [%], (b) contribution of categories to the total amount [%] and (c) deviation of occurence [%] in the tuned experiment from the control experiment.

of the high ones in the tuned experiment result from the shift of the autoconversion frequency from lower to higher values (see Section 3.5.1). Because of the importance of the autoconversion process in warm clouds which accounts for more than 70% of the rain occurrence in the Tropics (Lau and Wu, 2003) and also in temperate zones dominated by frontal systems, the impact of the tuned version of the new autoconversion parameterization on the large-scale precipitation is analyzed for these regions separately in the following section.

In temperate zones considered as the regions between $60°\text{S}-30°\text{S}$ and $30°\text{N}-60°\text{N}$, the control experiment exhibits in the first two categories, containing the artificially produced and non-measurable precipitation, frequencies of 43.4% and 12.4% (Fig. 3.13a) which are lower than the global mean (Fig. 3.12a). In the low, moderate and high precipitation categories the frequencies of 27.6%, 14.9% and 1.6% are higher in the temperate zones than the global mean (Fig. 3.13a). Thus, the contribution of low precipitation rates to the total amount is lower and the one of high rates higher in the temperate zone (Fig. 3.13b). The tuned autoconversion scheme causes a clear reduction of low precipitation rates by -11%, a strong increase of 21.1% of the non-measurable ones and

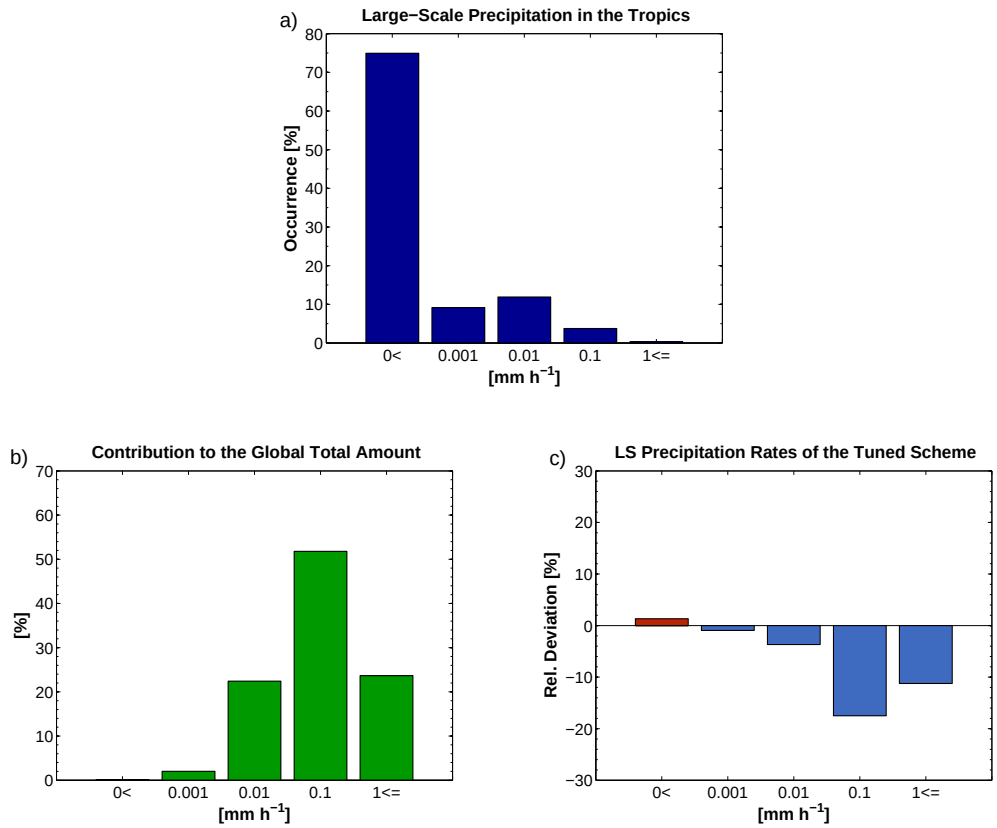

Figure 3.14.: Large-scale precipitation in the Tropics: (a) occurrence of precipitation rates by categories in the control experiment [%], (b) contribution of categories to the total amount [%] and (c) deviation of occurence [%] in the tuned experiment from the control experiment.

a slight increase of the moderate and high precipitation rates compared to the control experiment (Fig. 3.13c). Altogether, the global trend of the shift of frequencies from low precipitation rates to high rates is also found in the temperate zones.

In the Tropics, defined as region between 30°S/N, the control experiment exhibits artificially produced precipitation of 74.9% being considerably higher than in the temperate zones, and non-measurable rates of 9.2%, being lower than the global mean (Fig. 3.14a) . The occurrence of low, moderate and high precipitation rates are also lower with frequencies of 11.9%, 3.7% and 0.3%, respectively. Note that in the Tropics, most precipitation forms due to convection. Noticeable changes in the contribution of the categories in this region compared to the global mean are observed in the low, moderate and high precipitation rates (Fig. 3.14b). Low rates contribute more, moderate and high rates less to the total amount of large-scale precipitation. Applying the tuned autoconversion scheme, the low, moderate and high precipitation rates are all decreased compared to the control experiment. Against the global trend, the moderate and high rates are clearly lower with -17.5% and -11.2%, respectively (Fig. 3.14c). This is mainly caused by the decreased LWP

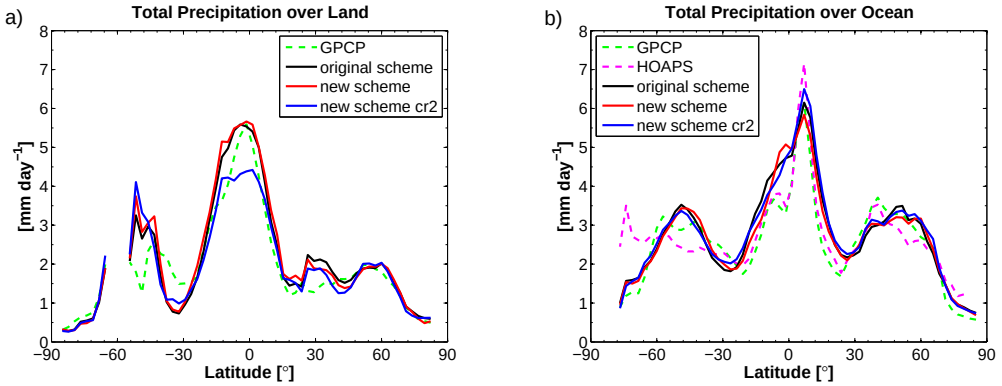

Figure 3.15.: Comparison between the zonal annual mean of total precipitation [mm day^{-1}] over land (a) and ocean (b) simulated by ECHAM5 with the original autoconversion as well as the untuned ("new scheme") and tuned ("new scheme $cr2$") version of the new autoconversion scheme, and HOAPS and GPCP data.

(and consequently decreased total cloud cover) in the stratocumulus regions in the western parts of the continents (see Fig. B.1) producing most of the large-scale precipitation in the Tropics. The artificially produced and non-measurable precipitation rates show only slight changes compared to the control experiment. The decrease in accumulated precipitation is compensated by convective precipitation (figure not shown).

3.5.7. Total Precipitation

A comparison of the changes in large-scale precipitation with observational data on a global scale is only possible by considering the total precipitation which includes the convective precipitation as well. Furthermore, the comparison is divided into a land and ocean analysis since the reference satellite dataset, HOAPS, provides only precipitation data over the ocean, whereas the GPCP dataset contains both land and ocean data.

The untuned version of the new scheme leads to a slight reduction of the global mean total precipitation by -0.8% and the tuned version by -1.7% relative to the control experiment with 0.121 mm h^{-1}. Whereas, the reduction of the global mean total precipitation in the tuned experiment is caused by both large-scale and convective precipitation, the reduction in the untuned experiment is caused only by large-scale precipitation. These findings may be a result of the slightly decreased occurrence of autoconversion caused by the new parameterization.

The total precipitation over land simulated in the untuned experiment is mostly somewhat higher than in the control experiment, except for $25°$N$-50°$N where it is lower (Fig. 3.15a). In the tuned experiment ($cr2$), the total precipitation is higher between $55°$S$-45°$S and around $35°$S and $55°$N, but considerably lower in the inner Tropics ($15°$S$-15°$N) and somewhat lower between $25°$N$-50°$N. In detail, the reduction of the total precipitation in the inner Tropics is more caused

by modeled convective than by the large-scale precipitation (Fig. B.2a/b). However, both kinds of precipitation over land depend, apart from the local evaporation, on the humidity advection from the ocean which is decreased so that more precipitation is modeled over the ocean rather than over land at the equator in the tuned experiment. Small improvements compared to the observational GPCP data are achieved around $35°$S and $30°$N in the tuned experiment.

The modeled total precipitation in the untuned and tuned experiment over the ocean shows only small differences compared to control experiment (Fig. 3.15b). In the untuned experiment, the total precipitation is mostly slightly lower, except between $50°\text{S}-30°\text{S}$ and around $5°$S where it is higher. The tuned experiment simulates somewhat higher total precipitation around $30°$S/N as well as at the equator and lower one between $5°\text{S}-15°\text{S}$. The assessment of improvements compared observational data over the ocean is quite difficult since both datasets are often different. However, the total precipitation in the untuned and tuned experiment are closer to both datasets in small regions between $15°\text{S}-5°\text{S}$ and around $30°$S.

3.6. Summary and Conclusions

A revised continuous autoconversion parameterization for warm clouds in a GCM accounting for the subgrid-scale variability of cloud liquid water was presented. The new parameterization combines the autoconversion by Beheng (1994) with the statistical approach developed by Tompkins (2002) using an integral of the autoconversion rate over the saturated part of the PDF of total water mixing ratio. The new scheme was implemented and applied in the ECHAM5 climate model in order to evaluate the impact of subgrid-scale variability of cloud liquid water on the autoconversion process. For this purpose model experiments with a horizontal resolution of T42 and 19 vertical levels were carried out using the prescribed sea surface temperature and sea ice distribution of 2004. Results obtained by the new autoconversion scheme were compared with the ones by the original parameterization considering the autoconversion rate and the affected quantities accretion rate, vertically integrated cloud liquid water, total cloud cover, CRF, large-scale precipitation and total precipitation. Moreover, total cloud cover and column liquid cloud water derived from MODIS, CRF from CERES EBAF satellite instruments and precipitation measurements from the HOAPS and GPCP datasets were used to asses the simulated quantities.

The results show that accounting for subgrid-scale variability of cloud liquid water in the autoconversion process leads to an increase of occurrence in higher autoconversion rates and to a reduction of lower ones compared to the parameterization using the mean cloud liquid water. This can be explained with the applied PDF of total water mixing ratio simulating the distribution of cloud liquid water in a model grid-box more realistically, i.e. emphasizing specific areas of cloud liquid water (single clouds). An analysis of the ratio of the new and original autoconversion rates reveals that the new autoconversion produces higher rates in all configurations of skewness and saturated parts of the PDF. In particular in cases with low cloud fraction, the new autoconversion rate can be up to 55 times higher than the original scheme.

Moreover, theoretical aspects of negative skewness affecting the new autoconversion rate were discussed considering the various configurations of the shape-parameters p and q and the saturated parts of the PDF. Although in the current version of the scheme only symmetric or positive skewness is allowed, in the future, it could be necessary also to allow negative skewness to obtain results being closer to observations (Chapter 2). A negatively skewed PDF simulates, depending on the saturation vapor mixing ratio, more clouds than areas with dry air, i.e without clouds, in a model grid-box. Also in that case, the new autoconversion parameterization generates higher amounts of cloud liquid water, and consequently higher autoconversion rates, which increases the more the PDF is skewed and saturated.

Additionally, the sensitivity of the new autoconversion scheme was tested varying the tuning factor in the autoconversion equation as well as the DW and skewness determining the shape of the PDF. To obtain a balanced net radiation flux at the TOA, the tuning factor could be decreased from 15 to 2 being actually closer to the factor 1 of original autoconversion parameterization derived by Beheng (1994). An increased DW leads to somewhat lower frequencies, but to a further shift of autoconversion rates to higher values. This finding can be regarded as important because the DW of the PDF is currently underestimated by the cloud cover scheme in the model related to observational data (Chapter 2). Therefore, a shift of the autoconversion to higher values will be likely when the deficiencies in the parameterization of DW are corrected.

Based on the fact that the skewness of the PDF is also flawed, i.e. it is clearly overestimated by the model, especially in the Tropics, the parameterization of the cloud cover scheme is used which was found to provide the closest results to observational data concerning the DW and skewness. This can be achieved by allowing negative skewness, reducing the dissipation of DW caused by vertical eddies, calculating skewness increase only for detrainment from ice-containing deep convection and general increasing of positive skewness (shape-parameter q) by 20% (Chapter 2). With this parameterization, the occurrence of higher autoconversion rates is considerably increased and shifted to higher rates. Although all sensitivity experiments produce some different distributions of autoconversion rates, they are clearly distinct compared to the one of the original autoconversion scheme. The observed increase of frequencies in higher autoconversion rates is not restricted to the parameterization by Beheng (1994). Similar results, but with a further increase of occurrence and a shift to higher autoconversion rates, were achieved applying the statistical approach to the parameterization developed by Khairoutdinov and Kogan (2000).

The modified autoconversion parameterization causes also a change in the distribution of accretion rates resulting from the coupling of both processes. The new distribution of the accretion rates resembles the one of the autoconversion rates with an increase of occurrence of higher rates and a decrease of lower ones compared to the original parametrization. Both autoconversion and accretion process affect directly the amount of cloud liquid water in the atmosphere. Applying the untuned version of the autoconversion scheme, the global mean vertically integrated cloud liquid water is decreased by -18% compared to the original scheme with $61\ \mathrm{g\ m^{-2}}$. However, the tuned autoconversion scheme leads to an increase of 34.4% in the LWP caused by the reduction of the tuning factor from 15 to 2. In the untuned experiment, the zonal annual mean of LWP is lower in all regions except around $60°\mathrm{N}$ compared to the control experiment. A general increase of LWP in all regions is obtained in the tuned experiment, which gives a better fit to the MODIS derived

column liquid cloud water compared to the original scheme. However, the LWP is somewhat overestimated around $60°$N by the tuned version of the new scheme compared to MODIS retrievals. Furthermore, a reduction of LWP is caused in the stratocumulus regions on the western parts of the continents relative to the control experiment in both versions of the new scheme. This has of course an impact of total cloud cover in these regions being also reduced.

On the global scale, the mean total cloud cover is decreased by -3.2% when the untuned autoconversion scheme is applied and increased by 1.6% using the tuned version compared to the original scheme with a mean total cloud cover of 0.63. These findings can be explained with a change similar to the one in LWP by the modified autoconversion process. The occurrence of total cloud fractions is also altered by the new autoconversion parameterization. An increase of total cloud fraction being lower than 0.5 and a decrease of fraction which is higher or equal to 0.5 are simulated in the untuned experiment compared to the control one. The opposite effect is obtained in the tuned experiment. Small differences of the zonal annual mean of total cloud cover are caused by both tuned and untuned autoconversion schemes relative to the original parameterization. However, in the Tropics, the cloud cover is somewhat lower in the untuned experiment. Improvements compared to the MODIS derived cloud cover are achieved between $45°\text{S}-25°\text{S}$ and $25°$N using the tuned autoconversion scheme.

The modified total cloud cover leads also to a change of SW CRF being -13% lower in the untuned experiment and increased by 1.5% in the tuned one compared to the control experiment with $-49.26\ \text{W m}^{-2}$. Regional differences can be seen in the zonal annual mean of the SW CRF. It is somewhat decreased between $60°\text{S}-60°$N, but considerably decreased in the inner Tropics ($15°\text{S}-15°$N) in the untuned experiment and somewhat increased around $50°$S and $60°$N in the tuned experiment compared to the control one. In general, a systematically better simulation of SW CRF related to the CERES EBAF measurements is not achieved applying either the untuned or the tuned version of the new autoconversion scheme. Only small differences in the LW CRF with -0.8% and 1.3% relative to the control experiment with $27.47\ \text{W m}^{-2}$ are obtained in the untuned and tuned experiment, respectively. Consequently, only slight improvements related to the CERES EBAF measurements are achieved around $60°$S and $10°$S in the untuned and around $30°$S/N in the tuned version of the the new scheme.

Simulated large-scale precipitation by the untuned autoconversion parameterization is almost equal to the global mean rate of the original parameterization with $0.047\ \text{mm h}^{-1}$. The tuned version of the new parameterization causes a reduction of the large-scale precipitation rate by -2.1% associated with a cooling of the land surfaces due to increased cloud cover. An analysis of the large-scale precipitation rates (hourly values) was carried out by considering five different categories of intensities. Because of the fact that there are no grid-boxes in the control experiment being exactly zero, the first category encompasses all grid-boxes having large-scale precipitation rates up to $0.001\ \text{mm h}^{-1}$. This category is regarded as artificially produced precipitation. It has an occurrence of 49.6%, but only a small contribution (0.1%) to the annual accumulated large-scale precipitation in the control experiment. The next category, encompassing the rates between $0.001 \leq P < 0.01\ \text{mm h}^{-1}$, has an occurrence of 15.4% and also a very low contribution (1.1%) to accumulated annual precipitation. Applying the new autoconversion parameterization (untuned and tuned version) increases the rates in both categories (the latter one more then the former).

Low precipitation rates being still measurable, for instance by radar instruments (Vali et al., 1998), are characterized by the category with rates between $0.01 \leq P < 0.1$ mm h^{-1}, which have an occurrence of 24.5% and contribute 16.5% to the accumulated annual mean large-scale precipitation in the control experiment. Moderate precipitation, defined as rates between $0.1 \leq P < 1.0$ mm h^{-1}, and high precipitation rates, larger equal than 1.0 mm h^{-1}, have an occurrence of 9.7% and 0.7%, respectively and contributions of 56% and 26.2% in the control experiment, respectively. The tuned version of the new autoconversion parameterization causes a reduction of -11.6% in the occurrence of low precipitation rates and an increase by 1.3% of high rates compared to the original parameterization. Moderate rates are slightly decreased by -0.8%. Similar results are obtained by the untuned experiment, except for the high precipitation rates being also slightly decreased by -0.6%. These findings can be explained by the shift of occurrence from low to higher autoconversion rates. The same trend (shift from low to high rates) in large-scale precipitation rates are observed in the temperate zones ($30^\circ - 60^\circ$S/N) in the tuned experiment. In the Tropics (30°S-30°N), against the global trend, the moderate and high rates are clearly lower with -17.5% and -11.2% in the tuned experiment, respectively. This is mainly a result of the decreased LWP (and consequently decreased total cloud cover) in the stratocumulus regions in the western parts of the continents producing the most large-scale precipitation in the Tropics.

A comparison of the changes in large-scale precipitation with observational data on a global scale was carried out regarding the total precipitation including also the convective precipitation. For this purpose, the HOAPS dataset providing precipitation data over the ocean and the GPCP dataset containing both land and ocean data are used. The untuned version of the new scheme leads to a marginal reduction of the global mean total precipitation by -0.8% and the tuned version by -1.7% compared to the original scheme with 0.121 mm h^{-1}. As expected, since the surface temperatures are held fixed, these changes are very small.

Small differences in zonal annual mean total precipitation simulated by the new autoconversion scheme relative to the original one are observed over land, except for the inner Tropics (15°S-15°N) where precipitation is substantially lower in the tuned experiment. The reduction of the total precipitation in the inner Tropics is more a result of the modeled convective than of the large-scale precipitation. Small improvements relative to the observational GPCP data are obtained around 35°S and 30°N in the tuned experiment. Over the ocean, the simulation of zonal annual total precipitation with the new scheme resembles the one of the original scheme. An assessment of the achieved improvements is quite difficult since the two observational datasets over the ocean differ often. However, the total precipitation in the untuned and tuned experiment are closer to both datasets in small regions between 15°S-5°S and around 30°S compared to the control experiment.

The incorporation of subgrid-scale variability of cloud liquid water into the autoconversion parameterization for warm clouds causes a shift of occurrence in large-scale precipitation from lower to higher rates. This result may lead to a reduction of the discrepancies between the occurrence of precipitation rates derived from CloudSat satellite retrievals and the modeled rates being overestimated for lower rates and underestimated for higher rates found by Nam (2010). The overly frequent occurrence of artificially-produced large-scale precipitation in ECHAM5 is probably a

result of deficiencies in the autoconversion parameterization and should therefore be further investigated. A formulation of the autoconversion dependent on a threshold may be solution here. Based on the knowledge that there are still differences between the modeled moments determining the PDF of total water mixing ratio and observations which have to be reduced, it is likely that the results achieved in this work will change in future. In particular, an increase of the DW of the PDF and allowing negative skewness in the model will cause a further shift to higher autoconversion rates, and potentially to higher large-scale precipitation rates.

4. Summary and Outlook

4.1. Summary

In this thesis, the representation of the subgrid-scale variability of total water in a GCM, and its impact on cloud microphysical processes such as formation of clouds and precipitation formation in warm clouds, i.e. autoconversion of cloud droplets, was investigated. The main focus in this work was set on the statistical PDF approach developed and implemented by Tompkins (2002) in the ECHAM5 climate model to take into account the horizontal subgrid-scale variability of total water within a model grid-box. The subgrid-scale variability scheme is used to calculate the horizontal cloud cover by integrating a beta-function based PDF of total water mixing ratio from the saturation vapor mixing ratio to the maximum of the total water mixing ratio. The temporal evolution of DW and skewness, varying the shape of the PDF, is expressed in terms of atmospheric processes such as convection, turbulence or precipitation formation.

In the first part of this thesis, the statistical cloud cover scheme was evaluated on the global scale by means of high-resolved satellite data. To achieve this, the mean variance and skewness in the GCM grid-box was derived for the TWP from retrievals by the MODIS satellite instrument. A one year simulation for two different model resolutions (T42L19 and T63L31) with prescribed sea surface temperature and sea ice of 2004 were carried out. Modeled total cloud cover, mean TWP as well as its variance and skewness were compared with the respective quantities derived from MODIS retrievals.

The findings show that the mean total cloud cover and the mean TWP are on average relatively well simulated. Differences were revealed in the spatial distribution of total cloud cover being underestimated by the model in the stratocumulus regions over the oceans off the western sides of the continents. The deviations of modeled TWP from the observations resemble the ones of the total cloud cover and seem to be caused by deficiencies of the hydrological cycle rather than by the cloud cover scheme. This is indicated by the RMSs in TWP for simulations by ECHAM5 with the statistical PDF scheme and relative humidity based cloud scheme (Sundqvist et al., 1989), which were found to be almost equal to each other. However, large deficiencies were found by the evaluation for both variance and skewness of the PDF. Skewness of TWP is strongly overestimated by the model in the Tropics, and underestimated in the extratropical regions. The main source of these discrepancies can be attributed to the model restriction which allows only symmetric or positively skewed PDFs, whereas the satellite data shows frequently also negative skewness, in particular in the Tropics. Systematically negative deviations of variance were analyzed for almost all regions of the globe. This may possibly be caused by the neglect of negative skewness, or by the precipitation process removing too much liquid water from clouds within one timestep.

The afore-mentioned patterns exist for both analyzed resolutions, where the coarser one has a somewhat smaller RMS of TWP, a somewhat higher RMS of its skewness, and a considerably larger RMS of its variance. The RMSs of total cloud cover are almost equal in both resolutions as well as in ECHAM5 configurations applying the PDF based cloud scheme and applying the optional relative humidity based cloud scheme.

For improvements of the statistical cloud cover scheme, the atmospheric processes affecting the variance and skewness were analyzed. For this purpose, some sensitivity experiments were made to adjust the parameterization of these statistical quantities varying the strength of dissipation and modifying the calculation of the temporal evolution of skewness. The strongest increase of variance is achieved by reducing the dissipation of DW caused by vertical eddies. A smaller impact on variance was found for the dissipation of DW caused by horizontal eddies and the vertical diffusion of DW. The large positive bias in the modeled skewness in the Tropics could be considerably reduced when the increase in skewness by convective detrainment was calculated only for deep convection revealing deficiencies in the link to the convection parameterization in the scheme. A further reduction of the bias in this region could be obtained allowing for negative skewness in the scheme using a relation between the two shape-parameters of the PDF suggested by Tompkins (2008). Applying this modification, the model is able to produce mean negative skewness mainly in the high and mid-latitudes, but still positive skewness in the Tropics. However, the closest results of modeled skewness and variance to observations can be achieved in combination of allowing negative skewness, calculating skewness increase only for detrainment from ice-containing deep convection, generally increasing positive skewness (shape-parameter q) by 20% and reducing the dissipation of DW caused by vertical eddies. The results show that the statistical PDF approach applied in the cloud cover scheme works in principle, but its parameterization has to be further improved in the future.

In the second part of the thesis, the impact of the subgrid-scale variability of cloud liquid water on the autoconversion process was analyzed. For this purpose, the statistical PDF approach by Tompkins (2002) was used to incorporate the subgrid-scale variability of cloud liquid water in the continuous autoconversion parameterization derived by Beheng (1994). The revised autoconversion parameterization was implemented in the cloud module of the ECHAM5 climate model. It now calculates the autoconversion process by an integral of the autoconversion rate over the saturated part of the PDF of total water mixing ratio. For the analysis, a one year simulation with the model resolution T42L19 was carried out using the prescribed sea surface temperature and sea ice distribution of 2004. The two different autoconversion schemes were compared considering the autoconversion rate as well as the affected quantities such as accretion rate, vertically integrated cloud liquid water, total cloud cover, CRF, large-scale precipitation and total precipitation. To evaluate the simulated quantities, total cloud cover and column liquid cloud water derived from MODIS, CRF from CERES EBAF satellite data and precipitation measurements from the HOAPS and GPCP datasets were utilized.

It was found that the introduction of the subgrid-scale variability of cloud liquid water into the autoconversion process causes an increase of occurrence in higher autoconversion rates and a reduction of lower ones compared to the original parameterization using the mean cloud liquid water. This result can be explained by the applied PDF of total water mixing ratio which emphasizes spe-

cific areas of cloud liquid water (single clouds). In general, the new autoconversion rate is for all configurations of the shape-parameter q and saturated part of the PDF higher than the original one, especially in cases with low cloud fraction, by a factor up to 55.

For improvements of the statistical PDF scheme, it could be helpful to allow also negative skewness in the scheme. In that case, the new autoconversion parameterization would produce higher amounts of cloud liquid water, and consequently higher autoconversion rates, which increases the more the PDF is skewed and saturated.

In line with sensitivity experiments, it was shown that the "tuning" factor in the autoconversion parameterization can be decreased from 15 to 2 to obtain a balanced net radiation flux at the TOA, and that an increased DW leads to a shift of autoconversion rates to higher values compared to the original one. Moreover, the parameterization of the statistical cloud cover scheme producing the closest results to observational data concerning the skewness and DW increases considerably the occurrence of higher autoconversion rates and moves them to higher rates. A further increase of occurrence in autoconversion rates is simulated when the current autoconversion formulation is replaced by the one developed by Khairoutdinov and Kogan (2000). This shows that the observed effect of the incorporated subgrid-scale variability of cloud liquid water is not restricted to the autoconversion parameterization derived by Beheng (1994).

The modified autoconversion process also causes an increase in occurrence of higher accretion rates and a decrease in lower ones due to the coupling between the parameterizations. Simulated vertically integrated cloud liquid water, and accordingly the total cloud cover, are slightly increased by the untuned autoconversion parameterization and decreased by the tuned one compared to the original scheme. However, both versions of the new autoconversion scheme lead to a reduction of LWP and total cloud cover in the stratocumulus regions over the ocean off the westerns sides of the continents. A better fit of zonal mean LWP and a small improvement of the zonal mean total cloud cover compared to observations are obtained in the tuned experiment. SW and LW CRF changed through the altered total cloud cover show slight improvements compared to observations applying the new autoconversion parameterizations.

The increase in occurrence of higher autoconversion rates and the reduction of lower ones cause globally a shift from lower large-scale precipitation rates ($0.01 \leq P < 0.1$ mm h^{-1}) to higher ones (1.0 mm h$^{-1} \leq P$). This trend was mainly found in the temperate zones ($30^\circ - 60^\circ$S/N), but not in the Tropics (30°S-30°N) where the occurrence of higher precipitation rates is also decreased. The reduction in this region can be attributed to the decreased LWP (and consequently decreased total cloud cover) in the stratocumulus regions in the western sides of the continents producing the most large-scale precipitation in the Tropics. Artificially produced very light precipitation in the model was not reduced by the new autoconversion parameterization, but even slightly increased. A comparison between modeled total precipitation (large-scale and convective precipitation) of the new and original autoconversion scheme and observations shows only small improvements. The considerably decreased precipitation in the Tropics in the tuned experiment is more a result of the modeled convective than the large-scale precipitation.

In summary, the incorporated subgrid-scale variability of cloud liquid water in the autoconversion process provides the expected shift of occurrence in large-scale precipitation from lower to higher rates and works basically. However, a further shift to higher autoconversion rates, and to higher large-scale precipitation rates, will be likely when the deficiencies in the parameterization of the PDF of total water mixing ratio are fixed.

4.2. Outlook

To achieve a better agreement of the modeled variance (distribution width) and skewness of TWP with observational data, the prognostic equations of these quantities should be revised, and the assumed beta-function based PDF could be replaced (e.g. by a bimodal or triangular PDF). In the current parameterization, vertical downdrafts transporting dry air from the upper atmosphere in the PBL and producing negative skewness, are not taken into account in the prognostic equation of skewness. The presence of negatively skewed distributions of total water mixing ratio in stratocumulus clouds was proved in various cloud cases with LESs by Zhu and Zuidema (2009) consistent with the observation-based findings in this thesis. Furthermore, Zhu and Zuidema showed that the variance of temperature can be equally important in controlling subgrid-scale clouds. Therefore, the introduction of negatively skewed PDFs and the inclusion of the subgrid-scale variability of temperature being currently neglected may potentially improve the scheme.

Based on the fact that the existing statistical PDF scheme produces different results depending on the model resolution, investigations should be pursued to develop a scale-independent parameterization for a statistical PDF scheme. For this purpose, ground based measurements (e.g. usage of LIDAR instruments) and high-resolved model experiments can be used to describe the influence of the various atmospheric processes on skewness and variance better or even find a more suitable or simpler PDF to apply. Finally, it also seems to be reasonable to develop a statistical PDF scheme which accounts for the vertical subgrid-scale variability of clouds being often neglected in GCMs. Since radiation is sensitive to cloud subgrid-scale variability, it would be valuable to continue investigations on the application of the cloud subgrid-scale variability scheme for radiative transfer (e.g. Räisänen and Järvinen, 2010) and thus improving climate simulations.

The revealed deficiencies in the current statistical PDF scheme affect also the new autoconversion parameterization, which exploits the PDF of total water mixing ratio to calculate the autoconversion rate. Implementing the suggested modifications listed above in the cloud cover scheme, a further shift of occurrence in autoconversion and therefore also in large-scale precipitation from lower to higher rates will be likely. The changes in the frequency of intensities in precipitation rates achieved in this study as well as the ones that will be obtained by future modifications should be compared with precipitation rates derived from CloudSat satellite retrievals using the method by Nam (2010).

As analyzed in this work, the ECHAM5 climate model has an overly frequent occurrance of very low artificially-produced large-scale precipitation, which is probably a result of the applied continuous autoconversion parameterization in this model. One possible solution to avoid this effect

can be the application of an autoconversion parameterization using a threshold to suppress the low artificially-produced precipitation.

The precipitation formation has also a major effect on the concentration of aerosols in the atmosphere. Aerosols are washed out when cloud droplets containing aerosol particles as condensation nuclei grow to raindrops or they are removed when collected by falling raindrops. Thus, the new autoconversion parameterization, and consequently the altered frequencies in large-scale precipitation, will probably also cause changes in simulated aerosol concentrations. This can be investigated in large-scale climate models containing special aerosol modules (e.g. HAM for ECHAM5). Another aspect being worth to analyze is the impact of the modified autoconversion parameterization on the climate sensitivity. This could be done with long-term model experiments using disturbed sea surface temperatures and evaluation of the resulting change of the global mean surface temperature. After introducing the subgrid-scale variability of clouds in the cloud formation and autoconversion process (indirectly also in the accretion process), the next logical step would be to implement the statistical PDF approach also in the growth processes of snow (aggregation of ice crystals, collecting ice crystals and cloud droplets).

A. Notes on Implementation of the New Autoconversion Scheme

The autoconversion process is implemented in the cloud module, where cloud microphysics such as condensation and evaporation is determined. These processes have strong impact on the bulk of cloud liquid water affecting the autoconversion rate. Since these processes are calculated before the autoconversion rate is computed, the in-cloud water is not anymore consistent with skewness and DW of TWC and cloud fraction. Consequently, there is a need to recompute these quantities to obtain consistency for the use in the autoconversion scheme.

Moreover, in the original autoconversion scheme, the calculation of the autoconversion rate and the time-integration are implicitly solved. Both procedures had to be separated using the Runge-Kutta method third-order for the time-integration before the implementation could be carried out. The third-order of the Runge-Kutta method was chosen because it gives the closest results to the formerly applied implicit time-integration compared to the first and second-order method. Subsequently, the model was fine-tuned using the constraint that at most 90% of the cloud liquid water can be converted to precipitation in one timestep to get the same results as with the original model parameterizations.

A crucial point was to find an applicable integration method, which was easy to implement into code and had low computational costs. The Simpson's rule is a method for a numerical integration approximating a definite integral. Some tests of this method with different shapes of the PDF resulted a good approximation with an error lower than 1% using 100 supporting points. Because of the third-order Runge-Kutta time-integration, the integration of the saturated part of the PDF of TWC has to be calculated three times. After each calculation, it is necessary to re-estimate the defining quantities (TWC, its maximum and its skewness) of the PDF using the equations introduced by Tompkins (2002). A change of cloud condensate Δr_c^{mic} due to the autoconversion process results a change of the maximum of TWC

$$\Delta b^{mic} = \frac{\Delta \overline{r}_c^{mic}}{\overline{r}_c} (b - r_s) \tag{A.1}$$

with

$$\Delta \overline{r}_c^{mic} = \overline{r}_{c,n+1}^{mic} - \overline{r}_{c,n}^{mic}, \tag{A.2}$$

where b is the maximum of TWC, r_s the saturation mixing ratio (always equal higher to the minimum of TWC a in cloudy situations considered here) and r_c the cloud condensate. The index 1 below r_c^{mic} represents the new mean cloud condensate after the first time-integration.

Afterwards, Δb^{mic} and the new TWC $\overline{r}_{t,n+1}$ are used to calculate the new shape-parameter q_{n+1}

$$q_{n+1} = \frac{\left(b + \Delta b^{mic} - a\right) p}{\overline{r}_{t,n+1} - a} - p. \tag{A.3}$$

p is the shape-parameter being set constant equal 2 and b the quantity containing the value before the time-integration. Then, the new b_{n+1} can be estimated

$$b_{n+1} = \left(\overline{r}_{t,n+1} - a\right) \frac{p + q_{n+1}}{p} + a. \tag{A.4}$$

After the last time-integration, the autoconversion rate is divided by cloud fraction of the respective grid-box to relate the rate to the cloud.

B. Supplementary Figures

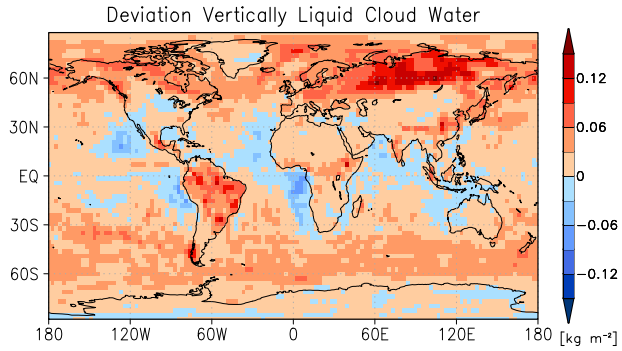

Figure B.1.: Deviation of vertically integrated cloud liquid water, simulated in the tuned experiment, from the control experiment [kg m^{-2}].

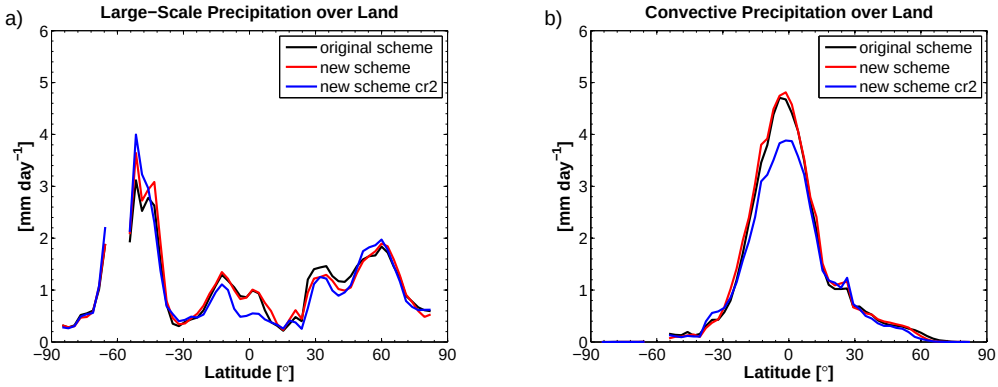

Figure B.2.: Comparison between the zonal annual mean of large-scale (a) and convective (b) precipitation [mm day^{-1}] over land simulated by ECHAM5 with the original autoconversion as well as the untuned ("new scheme") and tuned ("new scheme *cr*2") version of the new autoconversion scheme.

C. Supplementary Tables

Table C.1.: First order moments of the statistical PDF scheme compared to the ones of the relative humidity scheme (model minus observation)

	Total Cloud Cover			**TWP** $\left[\mathbf{kg\,m^{-2}}\right]$		
Experiment	Bias	RMS	Rel. Err.	Bias	RMS	Rel. Err.
T42L19 PDF	0.02	0.14	3.2%	0.34	3.34	1.3%
T42L19 rel. hum.	0.02	0.13	3.2%	0.68	3.46	2.6%
T63L31 PDF	0.03	0.13	4.8%	0.48	3.43	1.8%
T63L31 rel. hum.	0.02	0.13	3.2%	0.69	3.44	2.6%

Table C.2.: First order moments of the statistical PDF scheme in different sensitivity experiments (model minus observation)

	Total Cloud Cover			**TWP** $\left[\mathbf{kg\,m^{-2}}\right]$		
Experiment	Bias	RMS	Rel. Err.	Bias	RMS	Rel. Err.
control	0.01	0.17	1.6%	-0.39	5.39	-1.5%
vdiff	0.02	0.17	3.1%	-0.04	4.40	-0.2%
vedd	0.00	0.17	0.0%	-0.44	4.52	-1.7%
hedd	0.01	0.17	1.6%	-0.02	4.54	-0.1%
rsk	0.02	0.17	3.1%	-0.09	4.74	-0.4%
qmin	-0.09	0.22	-14.1%	-0.31	4.98	-1.2%
pvar	-0.02	0.18	-3.1%	-0.36	5.19	-1.4%
rsk+vedd	0.00	0.18	0.0%	-0.54	4.96	-2.1%
rsk+vedd+pvar	-0.09	0.24	-14.1%	-0.91	5.23	-3.6%
rsk+vedd+pvar+skew	-0.03	0.20	-4.7%	-0.39	5.06	-1.5%

Table C.3.: High order moments of the statistical PDF scheme in different model resolutions (model minus observation)

	Skewness			**Skewness (30°S-30°N)**			**Variance** $\left[\mathbf{kg^2\,m^{-4}}\right]$		
Experiment	Bias	RMS	Rel. Err.	Bias	RMS	Rel. Err.	Bias	RMS	Rel. Err.
T42L19 PDF	0.01	0.49	5.0%	0.23	0.40	460.0%	-6.20	10.15	-82.0%
T63L31 PDF	0.00	0.41	0.0%	0.19	0.35	316.7%	-4.07	6.85	-78.3%

Table C.4.: High order moments of the statistical PDF scheme in different sensitivity experiments (model minus observation)

	Skewness			**Skewness (30°S-30°N)**			**Variance** $\left[\mathbf{kg^2\,m^{-4}}\right]$		
Experiment	Bias	RMS	Rel. Err.	Bias	RMS	Rel. Err.	Bias	RMS	Rel. Err.
control	-0.09	0.72	-31.0%	0.20	0.44	333.3%	-6.03	10.66	-82.9%
vdiff	-0.08	0.73	-27.6%	0.22	0.45	366.7%	-6.05	10.64	-83.2%
vedd	-0.04	0.73	-13.8%	0.25	0.47	416.7%	-4.45	9.47	-61.2%
hedd	-0.07	0.73	-24.1%	0.23	0.47	383.3%	-5.94	10.54	-81.7%
rsk	-0.23	0.69	-79.3%	-0.03	0.30	-50.0%	-5.38	10.05	-74.0%
qmin	-0.49	0.92	-169.0%	-0.15	0.50	-250.0%	-5.76	10.39	-79.2%
pvar	-0.23	0.81	-79.3%	0.10	0.47	166.7%	-4.70	9.77	-64.6%
rsk+vedd	-0.23	0.69	-79.3%	-0.04	0.30	-66.7%	-3.34	8.84	-45.9%
rsk+vedd+pvar	-0.48	0.80	-165.5%	-0.32	0.44	-533.3%	-3.74	9.11	-51.4%
rsk+vedd+pvar+skew	-0.16	0.68	-55.2%	0.00	0.32	0.0%	-4.11	9.35	-56.5%

Table C.5.: Global annual mean values of quantities in different experiments (see text for descriptions of the experiments) and their relative devations from the control experiment.

	Experiments										
	control	**new scheme**		**cr2**		**vedd**		**nqx2**		**kk**	
Quantity	Mean	Mean	Dev.	Mean	Dev.	Mean	Dev.	Mean	Dev.	Mean	Dev.
Autoconv. Rate [μg kg^{-1}s^{-1}]	22.9	9.4	-58.7%	6.1	-73.4%	18.6	-18.8%	84.3	268.1%	14.9	-34.9%
Autoconv. Rate [μg kg^{-1}s^{-1}] (cldy)	53.1	24.6	-53.7%	14.4	-72.9%	43.4	-18.3%	197.9	272.7%	45.4	-14.5%
Accretion Rate [μg kg^{-1}s^{-1}]	3.7	12.4	235.1%	9.3	151.4%	16.6	348.6%	21.8	489.2%	16.2	337.8%
Accretion Rate [μg kg^{-1}s^{-1}] (cldy)	9.9	33.4	237.3%	22.7	129.3%	46.7	371.7%	55.8	463.6%	45.8	362.6%
LWP [g m^{-2}]	61	50	-18.0%	82	34.4%	48	-21.3%	21	-65.6%	57	-6.6%
Total cloud cover [fraction]	0.63	0.61	-3.2%	0.64	1.6%	0.59	-6.3%	0.53	-15.9%	0.60	-4.8%
SW CRF [W m^{-2}]	-49.26	-42.86	-13.0%	-50.00	1.5%	-40.75	-17.3%	-28.62	-41.9%	-39.25	-20.3%
LW CRF [W m^{-2}]	27.47	27.24	-0.8%	27.84	1.3%	27.17	-1.1%	26.26	-3.1%	26.75	-2.6%
Large-Scale Precip. [mm h^{-1}]	0.047	0.047	0.0%	0.046	-2.1%	0.048	2.1%	0.049	4.3%	0.047	0.0%
Convective Precip. [mm h^{-1}]	0.074	0.073	-1.4%	0.073	-1.4%	0.071	-4.1%	0.069	-6.8%	0.072	-2.7%
Total Precipitation [mm h^{-1}]	0.121	0.120	-0.8%	0.119	-1.7%	0.119	-1.7%	0.118	-2.5%	0.119	-1.7%

List of Abbreviations

AMIP	Atmospheric Model Intercomparison Project
CAPE	convective potential energy
CERES	Clouds and the Earth's Radiant Energy System
CRF	cloud radiative forcing
CRM	cloud resolving model
DW	distribution width
EBAF	Energy Balanced and Filled
ECHAM5	general circulation model version 5 developed at MPI-M
GCM	general circulation model
GPCP	Global Precipitation Climatology Project
HIRHAM	a regional atmospheric climate model
HOAPS	Hamburg Ocean Atmosphere Parameters and Fluxes from Satellite Data
LES	large-eddy simulation
LIDAR	light detection and ranging
LW	longwave
LWP	column liquid cloud water
MODIS	Moderate Resolution Imaging Spectroradiometer
MPI-M	Max Planck Institute for Meteorology
PBL	planetary boundary layer
PDF	probability density function
RMS	root mean square error
RRTM	Rapid Radiative Transfer Model
SCM	single column model
SW	shortwave
TOA	top of the atmosphere
TWP	total water path

List of Figures

List of Tables

Acknowledgements

This page is dedicated to all persons who supported this work and made this thesis possible. I thank Johannes Quaas for being an excellent supervisor, for his scientific advice and guidance and the continuous support throughout the last years. I sincere thanks to Martin Claußen for the academic supervision of this work, for his interest and being my panel chair. I am very thankful to Erich Roecker, who contributes with his experience and his huge knowledge of the ECHAM5 model so much to this work. A special thank goes to Sebastian Rast for providing the subroutines for integrating the probability density function and the helpful manual of ECHAM5 as well as for his programming support. I would like to thank the members of Cloud-Climate Feedback Group and my office roommates for their useful discussions and for the comfortable atmosphere. I am very grateful to Verena Grützun and to all the other reviewers for proofreading the manuscript and for their constructive comments.

My PhD work was funded by the German Research Foundation (Deutsche Forschungsgemeinschaft, DFG) by an “Emmy Noether” grant and was done in the framework of the International Max Planck Research School on Earth System Modelling (IMPRS-ESM). Many thanks go to Antje Weitz and Cornelia Kampmann for their administratively and morally support. These simulations were carried out at the German High Performance Computing Centre for Climate- and Earth System Research (Deutsches Klimarechenzentrum, DKRZ). Finally, I also thank the CIS team for the technical support and the people in the administration of the Max Planck Institute for Meteorology for their help. At all times, I greatly enjoyed the friendly, cooperative, and inspiring atmosphere at the institute. I am deeply thankful to my family and my friends for their support and confidence.

Bibliography

Adler, R. F., Huffman, G. J., Chang, A., Ferraro, R., Xie, P.-P., Janowiak, J., Rudolf, B., Schneider, U., Curtis, S., Bolvin, D., Gruber, A., Susskind, J., Arkin, P., and Nelkin, E. (2003). The version-2 global precipitation climatology project (GPCP) monthly precipitation analysis (1979-present). *J. Hydrometeor.*, 4:1147–1167.

Andersson, A., Bakan, S., Fennig, K., Graßl, H., Klepp, C.-P., and Schulz, J. (2007). Hamburg ocean atmosphere parameters and fluxes from satellite data - HOAPS-3 - twice daily composite. *electronic publication*. World Data Center for Climate. doi:10.1594/WDCC/HOAPS3-DAILY.

Andersson, A., Fennig, K., Klepp, C., Bakan, S., Graßl, H., and Schulz, J. (2010). The hamburg ocean atmosphere parameters and fluxes from satellite data - HOAPS-3. *Earth Syst. Sci. Data Discuss.*, 3:143–194. doi:10.5194/ESSDD-3-143-2010.

Beheng, K. D. (1994). A parameterization of warm cloud microphysical conversion processes. *Atmos. Res.*, 33:193–206.

Boucher, O. and Treut, H. L. (1995). Precipitation and radiation modeling in a general circulation model: Introduction of cloud microphysical processes. *J. Geophys. Res.*, 100(D8):16395–16414.

Bretherton, C. S., Uttal, T., Fairall, C. W., Yuter, S. E., Weller, R. A., Baumgardner, D., Comstock, K., Wood, R., and Raga, G. B. (2004). The EPIC 2001 stratocumulus study. *BAMS*, 85(7):967–977.

Chen, C. and Cotton, W. R. (1987). The physics of the marine stratocumulus-capped mixed layer. *J. Atmos. Sci.*, 44:2951–2977.

Chen, C.-T., Roeckner, E., and Soden, B. J. (1996). A comparison of satellite observations and model simulations of column-integrated moisture and upper-tropospheric humidity. *J. Climate*, 9:1561–1585.

Cheng, A. and Xu, K.-M. (2009). A PDF-based microphysics parameterization for simulation of drizzling boundary layer clouds. *J. Atmos. Sci.*, 66:2317–2334. doi:10.1175/2009JAS2944.1.

Davis, A., Marshak, A., Wiscombe, W., and Cahalan, R. (1996). Scale invariance of liquid water distributions in marine stratocumulus. Part I: Spectral properties and stationary issues. *J. Atmos. Sci.*, 53(11):1538–1558.

Doutriaux-Boucher, M. and Quaas, J. (2004). Evaluation of cloud thermodynamic phase parameterizations in the LMDZ GCM by using POLDER satellite data. *Geophys. Res. Lett.*, 31:1–5. doi:10.1029/2003GL019095.

Fouquart, Y. and Bonnel, B. (1980). Computations of solar heating of the earth's atmosphere: A new parameterization. *Beitr. Phys. Atmos.*, 53:35–62.

Gates, W. L., Boyle, J. S., Covey, C., Dease, C. G., Doutriaux, C. M., Drach, R. S., Fiorino, M., Gleckler, P. J., Hnilo, J. J., Marlais, S. M., Phillips, T. J., Potter, G. L., Santer, B. D., Sperber, K. R., Taylor, K. E., and Williams, D. N. (1999). An overview of the results of the Atmospheric Model Intercomparison Project (AMIP I). *Bull. Amer. Meteor. Soc.*, 80(1):29–55.

Glickman, T. S. (2000). AMS Glossary of Meteorology. 2nd ed. *Amer. Meteor. Soc.*, page 855 pp.

Golaz, J.-C., Larson, V. E., and Cotton, W. R. (2002). A PDF-based model for boundary layer clouds. Part I: Method and model description. *J. Atmos. Sci.*, 59:3540–3551.

Houze, Jr., R. A. (1993). Cloud Dynamics. *Academics Press, Inc.*, page 605 pp.

Huffman, G. J., Adler, R. F., Bolvin, D. T., and Gu, G. (2009). Improving the global precipitation record: (GPCP) version 2.1. *Geophys. Res. Lett.*, 36:1–5. doi:10.1029/2009GL040000.

Jess, S. (2010). Impact of subgrid variability on large-scale precipitation formation in the climate model ECHAM5. PhD Thesis, 93 pp. ETH Zurich, Switzerland.

Khairoutdinov, M. and Kogan, Y. (2000). A new cloud physics parameterization in a large-eddy simulation model of marine stratocumulus. *Mon. Wea. Rev.*, 128:229–243.

King, M. D., Menzel, W. P., Kaufman, Y. J., Tanré, D., Gao, B.-C., Platnick, S., Ackerman, S. A., Remer, L. A., Pincus, R., and Hubanks, P. A. (2003). Cloud and aerosol properties, precipitable water, and profiles of temperature and water vapor from modis. *IEEE Transactions on Geoscience and Remote Sensing*, 41(2):442–458.

Lau, K. M. and Wu, H. T. (2003). Warm rain processes over tropical oceans and climate implications. *Geophys. Res. Lett.*, 30:1–5. doi:10.1029/2003GL018567.

LeTreut, H. and Li, Z.-X. (1991). Sensitivity of an atmospheric general circulation model to prescribed SST changes: Feedback effects associated with the simulation of cloud optical properties. *Clim. Dyn.*, 5:175–187.

Levkov, L., Rockel, B., Kapitza, H., and Raschke, E. (1992). 3D mesoscale numerical studies of cirrus and stratus clouds by their time and space evolution. *Betr. Phys. Atmos.*, 65:35–58.

Lin, S.-J. and Rood, R. B. (1996). Multidimensional flux-form semi-lagrangian transport schemes. *Mon. Wea. Rev.*, 124:2046–2070.

Lin, Y.-L., Farley, R. D., and Orville, H. D. (1983). Bulk parameterization of the show field in a

cloud model. *J. Clim. Appl. Meteor.*, 22:1065–1092.

Loeb, N. G., Wielicki, B. A., Doelling, D. R., Smith, G. L., Keyes, D. F., Kato, S., Manalo-Smith, N., and Wong, T. (2008). Toward optimal closure of the earth's top-of-atmosphere radiation budget. *J. Climate*, 22:748–766. doi:10.1175/2008JCLI2637.1.

Lohmann, U. and Roeckner, E. (1996). Design and performance of a new cloud microphysics scheme developed for the ECHAM general circulation model. *Clim. Dyn.*, 12:557–572.

May, W. (2008). Potential future changes in the characteristics of daily precipitation in europe simulated by the HIRHAM regional climate model. *Clim. Dyn.*, 30:581–603. doi:10.1007/s00382-007-0309-y.

Medeiros, B. and Stevens, B. (2011). Revealing differences in GCM representations of low clouds. *Clim. Dyn.*, 36:385–399. doi:10.1007/s00382-009-0694-5.

Mellor, G. L. (1977). The gaussian cloud relations. *J. Atmos. Sci.*, 34:356–358.

Mlawer, E. J., Taubman, S. J., Brown, P. D., Iacono, M. J., and Clough, S. A. (1997). Radiative transfer for inhomogeneous atmospheres: RRTM, a validated correlated-k model for the longwave. *J. Geophys. Res.*, 102:16663–16682. doi:10.1029/97JD00237.

Murakami, M. (1990). Numerical modeling of dynamical and microphysical evolution of an isolated convective cloud - the 19 july 1981 CCOPE cloud. *J. Meteor. Soc. Japan*, 68:107–128.

Nam, C. (2010). Using CALIPSO and CloudSat satellite retrievals to evaluate low-level cloud parameterizations in ECHAM5 for cloud-climate feedback implications. PhD Thesis in preparation. Max Planck Institute for Meteorology, Hamburg, Germany.

Nishizawa, K. (2000). Parameterization of nonconvective condensation for low-resolution climate models: Comparison of diagnostic schemes for fractional cloud cover and cloud water content. *Q. J. R. Meteor. Soc. Japan*, 78(1):1–12.

Nordeng, T. E. (1994). Extended versions of the convective parameterization scheme at ECMWF and their impact on the mean and transient activity of the model in the tropics. Technical Memorandum No. 206, ECMWF, Reading, UK. Available at http://www.ecmwf.int/publications.

Pincus, R., Hannay, C., Klein, S. A., Xu, K.-M., and Hemler, R. (2005). Overlap assumptions for assumed probability distribution function cloud schemes in large-scale models. *J. Geophys. Res.*, 110:1–12. doi:10.1029/2004JD005100.

Pincus, R., Hemler, R., and Klein, S. A. (2006). Using stochastically generated subcolumns to represent cloud structure in a large-scale model. *Mon. Wea. Rev.*, 134:3644–3656.

Pincus, R. and Klein, S. A. (2000). Unresolved spatial variability and microphysical process rates in large-scale models. *J. Geophys. Res.*, 105:27059–27065.

Platnick, S., King, M. D., Ackerman, S. A., Menzel, W. P., Baum, B. A., Riédi, J. C., and Frey, R. A. (2003). The MODIS cloud products: Algorithms and examples from terra. *IEEE Transactions on Geoscience and Remote Sensing*, 41(2):459–473.

Posselt, R. and Lohmann, U. (2008). Introduction of prognostic rain in ECHAM5: design and single column model simulations. *Atmos. Chem. Phys.*, 8:2949–2963.

Price, J. D. (2001). A study of probability distributions of boundary-layer humidity and associated errors in parameterized cloud-fraction. *Q. J. R. Meteorol. Soc.*, 127(573):739–758.

Räisänen, P., Barker, H. W., Khairoutdinov, M. F., Li, J., and Randall, D. A. (2004). Stochastic generation of subgrid-scale cloudy columns for large-scale models. *Q. J. R. Meteorol. Soc.*, 130:2047–2067. doi:10.1256/qj.03.99.

Räisänen, P. and Järvinen, H. (2010). Impact of cloud and radiation scheme modifications on climate simulated by the ECHAM5 atmospheric GCM. *Q. J. R. Meteorol. Soc.*, 136:1733–1752. doi:10.1002/qj.674.

Roeckner, E., Bäuml, G., Bonaventura, L., Brokopf, R., Esch, M., Giorgetta, M., Hagemann, S., Kirchner, I., Kornblueh, L., Manzini, E., Rhodin, A., Schlese, U., Schulzweida, U., and Tompkins, A. (2003). The atmospheric general circulation model ECHAM5 part I: Model description. *Max Planck Institute for Meteorology*. Report No. 349. Available at http://www.mpimet.mpg.de/fileadmin/publikationen/Reports.

Rotstayn, L. D. (1997). A physically based scheme for the treatment of stratiform clouds and precipitation in large-scale models. I: Description and evaluation of the microphysical processes. *Q. J. R. Meteorol. Soc.*, 123:1227–1282.

Rotstayn, L. D. (2000). On the "tuning" of autoconversion parameterization in climate models. *J. Geophys. Res.*, 105:15495–15507.

Schulz, J.-P., Dümenil, L., and Polcher, J. (2001). On the land surface-atmosphere coupling and its impact in a single-column atmospheric model. *J. Appl. Meteor.*, 40:642–663.

Seethala, C. and Horváth, A. (2010). Global assessment of AMSR-E and MODIS cloud liquid water path retrievals in warm oceanic clouds. *J. Geophys. Res.*, 115:1–19. doi:10.1029/2009JD012662.

Slingo, J. M. (1987). The development and verification of a cloud prediction scheme for the ECMWF model. *Q. J. R. Meteorol. Soc.*, 113:899–927.

Smith, R. N. B. (1990). A scheme for predicting layer clouds and their water content in a general circulation model. *Q. J. R. Meteorol. Soc.*, 116:435–460.

Sommeria, G. and Deardorff, J. W. (1977). Subgrid-scale condensation in models of nonprecipitating clouds. *J. Atmos. Sci.*, 34:344–355.

Sundqvist, H. (1978). A parameterization scheme for non-convective condensation including prediction of cloud water content. *Q. J. R. Meteorol. Soc.*, 104:677–690.

Sundqvist, H., Berge, E., and Kristjánsson, J. E. (1989). Condesation and cloud parameterization studies with a mesoscale numerical weather predicition model. *Mon. Wea. Rev.*, 117:1641–1657.

Tiedtke, M. (1989). A comprehensive mass flux scheme for cumulus parameterization in large-scale models. *Mon. Wea. Rev.*, 117:1779–1800.

Tompkins, A. M. (2002). A prognostic parameterization for the subgrid-scale variability of water vapor and clouds in large-scale models and its use to diagnose cloud cover. *J. Atmos. Sci.*, 59(12):1917–1942.

Tompkins, A. M. (2008). 'Cloud Parametrization'. *In Proceedings of Workshop on Parameterization of Subgrid Physics Processes, Reading, UK, 1-4, September 2008.* ECMWF, Reading, UK. Available at http://www.ecmwf.int/publications.

Vali, G., Kelly, R. D., French, J., Haimov, S., Leon, D., McIntosh, R. E., and Pazmany, A. (1998). Finescale structure and microphysics of coastal stratus. *J. Atmos. Sci.*, 55:3540–3564.

Watanabe, M., Emori, S., Satoh, M., and Miura, H. (2009). A PDF-based hybrid prognostic cloud scheme for general circulation models. *Clim. Dyn.*, 33:795–816.

Wood, R. and Field, P. R. (2000). Relationships between total water, condensed water, and cloud fraction in stratiform clouds examined using aircraft data. *J. Atmos. Sci.*, 57:1888–1905.

Wood, R., Field, P. R., and Cotton, W. R. (2002). Autoconversion rate bias in stratiform boundary layer cloud parameterization. *Atmos. Res.*, 65:109–128.

Xu, K.-M. and Randal, D. A. (1996). A semiempirical cloudiness parameterization for use in climate models. *J. Atmos. Sci.*, 53(21):3084–3102.

Zhang, J. and Lohmann, U. (2002). A new statistically based autoconversion reate parameterization for use in large-scale models. *J. Geophys. Res.*, 107(D24):1–16. doi:10.1029/2001JD001484.

Zhu, P. and Zuidema, P. (2009). On the use of PDF schemes to parameterize sub-grid clouds. *J. Geophys. Res.*, 36. doi:10.1029/2008GL036817.



ISSN 1614-1199